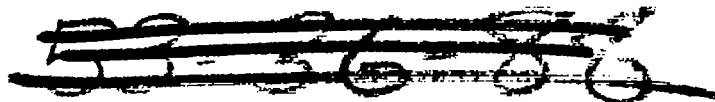


~~CONFIDENTIAL~~

Copy 217  
RM L54C08

NACA RM L54C08

7533



# RESEARCH MEMORANDUM

MEASUREMENTS AND PREDICTIONS OF FLOW CONDITIONS ON A  
TWO-DIMENSIONAL BASE SEPARATING A MACH NUMBER 3.36  
JET AND A MACH NUMBER 1.55 OUTER STREAM

By Donald E. Coletti

Langley Aeronautical Laboratory  
Langley Field, Va.

~~This material is the property of the National Advisory Committee for Aeronautics and is loaned to you for your use only. It is to be returned to the committee in the manner and by the date specified on the loan slip. The transmission or revelation of which in any manner to an unauthorized person is prohibited by law.~~

NATIONAL ADVISORY COMMITTEE  
FOR AERONAUTICS

WASHINGTON

May 7, 1954

~~CONFIDENTIAL~~

~~44-54-2117~~

Classification cancelled (or changed to UNCLASSIFIED)

By Authority of NASA Tech Rep Announcement # 13  
(OFFICER AUTHORIZED TO CHANGE)

By [Signature]  
NAME AND

[Signature]  
GRADE OF OFFICER MAKING CHANGE)

3 Apr 61  
DATE

B

NACA RM L54C08

~~CONFIDENTIAL~~

TECH LIBRARY KAFB, NM



0144339

NATIONAL ADVISORY COMMITTEE FOR AERONAUTICS

RESEARCH MEMORANDUM

MEASUREMENTS AND PREDICTIONS OF FLOW CONDITIONS ON A  
TWO-DIMENSIONAL BASE SEPARATING A MACH NUMBER 3.36  
JET AND A MACH NUMBER 1.55 OUTER STREAM

By Donald E. Coletti

SUMMARY

An investigation has been made in a mixing-zone apparatus to study the effects of jet flow on two-dimensional base pressure and the development of supersonic channel flow about a two-dimensional base, with and without splitter plates of different thicknesses. The Mach number of the outer streams ahead of the base was 1.55 for fully developed supersonic flow, whereas for the center jet the Mach number was 3.36.

The results of the investigation indicated that the semiempirical method presented in NACA RM L53C02 gave a good prediction of the pressure on a two-dimensional base separating supersonic streams of different Mach numbers, stagnation pressures, and static pressures. Also, the flow pattern downstream of the jet exit was predicted satisfactorily by the regular shock and expansion equations and two-dimensional characteristics. Within the limits of this investigation, the base-pressure coefficient is unchanged when the absolute magnitudes of the center-jet and outer-stream pressures are varied providing the ratio of the two pressures is constant. Without the center jet, there was little or no variation of the base pressure across the base. During the process of establishing supersonic flow in the outer stream, the base pressure was increased as much as 30 percent by the addition of the splitter plate; a very small increase was observed for a fully developed supersonic flow. This effect was due to the action of the splitter plate in decreasing the turbulent scavenging by preventing the formation of the large vortices of the Karman vortex street.

INTRODUCTION

Recently, considerable interest has centered upon the behavior of the flow about a base which separates a propulsive jet from an outer stream. Since this type of base is present in jet-propelled aircraft

~~CONFIDENTIAL~~

~~2/16/57-1143~~

and missiles, knowledge of the base drag and of possible methods for its prediction and alleviation is important.

For the case in which a jet issues from the base, reference 1 presents results from an investigation of jet effects on boattail and base pressures for axially symmetric configurations. For the case without jet flow, fair estimates of the drag may be made by the methods presented in references 2 to 4, provided the boundary layer ahead of the base is turbulent. The approach of reference 4, which considers most of the primary variables that affect base drag in the absence of jet flow, hinges upon the concept of the base pressure being primarily dependent upon the pressure rise required to separate the boundary layer. Reference 4 also discusses briefly an analogy between the angle-of-attack effects on the pressure on a two-dimensional base in a uniform stream and the pressure on a base separating supersonic streams having different Mach numbers and pressures. In order to examine further the possibility of predicting the pressure on the latter type of base configuration, the present investigation was conducted in the mixing-zone apparatus (MZA) of the Langley 9-inch supersonic tunnel.

A secondary purpose of the investigation was to study the flow downstream of a two-dimensional base spanning a supersonic channel, with particular emphasis on the effects of splitter plates on the flow during the process of establishing supersonic flow in the outer stream. The addition of a splitter plate to a two-dimensional base has been shown to reduce the base drag considerably (see refs. 5 to 7) by the elimination or suppression of the regular Karman vortex street. A somewhat similar action has been indicated by reference 8 to take place on a body of revolution when a sting is added to the base.

#### SYMBOLS

M	Mach number
$P_0$	stagnation pressure of outer streams, in. Hg abs
$P_j$	stagnation pressure of center jet, in. Hg abs
p	static pressure, in. Hg abs
$P_1$	outer-stream static pressure, in. Hg abs
$P_2$	center-jet static pressure, in. Hg abs
$P_b$	static pressure on base, in. Hg abs

$P_b$	base-pressure coefficient, $\frac{P_b - P_1}{q_1}$
$P_r$	pressure-rise coefficient required to separate a turbulent boundary layer
$h$	height of two-dimensional base or center jet, in.
$q_1$	outer-stream dynamic pressure, in. Hg abs
$x$	distance downstream from end of two-dimensional base, in.
$x_d$	distance to location of flow division on splitter plate, in.
$y$	distance from $h/2$ on two-dimensional base, in. (see fig. 6)
$z$	spanwise distance across width of mixing-zone apparatus, in.

#### APPARATUS AND TESTS

##### Mixing-Zone Apparatus

General description.- All tests were conducted in the supersonic mixing-zone apparatus (MZA) which is located in the Langley 9-inch supersonic tunnel building. Figure 1 presents a schematic drawing of the main components of the apparatus. This apparatus is of the blowdown type and utilizes the high-pressure air supply of the Langley 9-inch supersonic tunnel for operation; the test section exhausts to the atmosphere.

Two independent flow systems are incorporated: The primary system which supplies the air for the outer streams, and the secondary system which supplies the air for the center stream or jet. (See fig. 2.) The systems may be operated singly or simultaneously, depending on the nature of the tests. The secondary system is capable of supplying air for a center jet having a stagnation temperature from about room temperature to 650° F. The higher temperatures are obtained by means of an inertia heater. However, for this investigation, tests involving the center jet were limited to stagnation temperatures of about room temperature. Maximum stagnation pressure for the primary system is 250 lb/sq.in. and for the secondary system, 500 lb/sq. in. The incoming air from the storage tanks has a dewpoint of approximately -30° F.

Test section.- The apparatus is so designed that either two- or three-dimensional nozzles may be used and readily interchanged. For the

present tests, a two-dimensional setup was used as shown in figure 2. The outer-stream Mach number and the jet Mach number may be varied by changing the outer nozzle blocks and center-jet unit, respectively. The outer-stream Mach number was 1.55 in the present tests (fully developed supersonic flow); a survey of the outer stream at and just ahead of the base of the center-jet nozzle for the fully supersonic condition is shown in figure 3. The center-jet Mach number is assumed to be 3.36 from an average of the results of a survey made at the exit of the jet and shown in figure 4. Figure 4 also shows that Mach number gradients existed across the exit of the jet and schlieren observation of the jet flow also indicated disturbances. The disturbances are caused by imperfections in the machining of the center-jet nozzle. In most of the tests in which the center jet was inoperative, the center-jet exit was closed by means of a metal plate inserted flush with the exit. With the center jet inoperative, the setup is essentially that of a thick two-dimensional base immersed in a two-dimensional stream.

Schlieren system.- For qualitative-flow observations, a double-image schlieren system is available which simultaneously records two images on a single photographic negative with a single spark of the source light. One image indicates vertical density gradients; the other, horizontal density gradients. This schlieren system is particularly suited to investigations involving unsteady flows and transient density fields. The design of this system was based upon information given in reference 9.

Other units.- The mixing-zone apparatus and its component units are operated from the control panel shown in figures 5(a) and 5(b). Pressures are indicated on the multiple-tube mercury manometer and by precision laboratory pressure gages; these pressures are recorded by camera.

#### Tests

The stagnation pressure of the outer streams was varied from 30 to about 380 inches of mercury absolute; the average stagnation temperature was 50° F. The stagnation pressure of the center jet was varied from 30 to 922 inches of mercury absolute and the average stagnation temperature was 73° F. The dew point for both the outer streams and center jet was approximately -30° F. From the results presented in reference 10, little or no effect of water-vapor condensation would be expected at a Mach number of 1.55, whereas at a Mach number of 3.36 some condensation effects may be present. It is believed, however, that any such effects were not large enough to have an important influence on the results obtained at this Mach number.

The first series of tests involved the use of the outer streams only and no splitter plates. In a portion of these tests, measurements

were made of the base pressure with the jet exit open (hollow base) by means of orifice 8 as indicated in figure 6(a). Tests were then made with a base plate inserted flush in the jet exit and having orifices located as shown in figure 6(a) also. The sides of the plate were sealed; the top and bottom were not sealed and thus allowed the small gaps to act as pressure orifices vented to the common orifice 8. The pressure indicated by orifice 8 for this setup was, therefore, a mean value between the pressures at the  $\frac{y}{h/2} = \pm 0.9$  locations. Orifice 3 is located on the inner surface of the center-jet nozzle at  $x = -0.1$ . Since the base plate is 1/8 inch thick, the orifice is under the edge of the base plate and therefore corresponds to  $\frac{y}{h/2} = -0.9$ , but the pressure at this orifice would also be subject to some effect from the pressure at  $\frac{y}{h/2} = 0.9$ . Some additional pressure-distribution measurements for the outer stream were made by a measurement of the static pressures along the outer surface of the center-jet housing by means of the orifices located as shown in figure 7 (orifices 9 to 14).

The second series of tests again involved the use of the outer streams only but with the use of splitter plates  $\frac{1}{16}$ ,  $\frac{1}{8}$ , and  $\frac{1}{4}$  inch thick attached to the center of the base plate as shown in figure 6(b). Static pressures were measured as in the first series of tests and visual observations of the flow along the splitter plate and base plate were made by glueing tufts of cotton to these surfaces.

The third series of tests involved the use of the center jet operating with and without the outer streams. Static pressures were measured by means of orifices located as shown in figure 7.

Schlieren pictures were taken of the flow about the base with and without splitter plates and base plate and with both the center jet and outer streams operating simultaneously over the range of stagnation pressures investigated.

#### PRECISION

The maximum estimated error for the stagnation pressure is  $\pm 0.5$  inch of mercury absolute; for the base or static pressures this error is  $\pm 0.1$  inch of mercury absolute. The resulting accuracy for the Mach number in both the outer streams and center jet is  $\pm 0.012$ . The maximum variation of the stagnation temperature for a given run (30 to 60 seconds) was approximately 5° F. The accuracy for the base-pressure coefficient is  $\pm 0.01$ .

## RESULTS AND DISCUSSION

## Starting Cycle for Outer Streams Only

The results of the pressure measurements with and without base plate and splitter plates are presented in figures 8 to 10 for each orifice as the variation in the ratio of the static pressure to the stagnation pressure  $\frac{P}{P_0}$  with  $p_0$ . In figures 11(a) and 11(b) are shown the variations of base and static pressure with stagnation pressure for orifices 4 and 9.

With and without base plate (no splitter plate).- The results shown in figure 8 for the various orifices show that, for a given value of  $p_0$ , there is little variation in the ratio of  $\frac{P}{P_0}$  for the base across the face of the base plate. This condition is more readily indicated by figure 9 where the distribution across the base is presented for several values of  $p_0$ . Both figures show that, beyond a value of  $p_0$  of about 140 inches of mercury,  $\frac{P}{P_0}$  experiences almost no change, whereas from 30 (no flow) to 140 inches of mercury the decrease in  $\frac{P}{P_0}$  which must occur exhibits several peculiar variations, notably in the range of  $p_0$  from 60 to 100 inches of mercury. The results of figure 8(i) show that the variation of  $\frac{P}{P_0}$  with the base open is essentially the same as that with the base plate installed.

An explanation for the behavior of the base pressure with increasing  $p_0$  may be seen in figure 12 where double-image schlieren photographs are presented for varying values of  $p_0$ . As explained in the description of the schlieren system, the vertical- and horizontal-knife-edge images are taken simultaneously. When the flow first begins, the schlieren photographs show that a well-defined Karman vortex street forms behind the base. The large vortices are seen to dip well into the region behind the base ( $p_0 = 35.6$  inches of mercury). The resulting turbulent scavenging of the dead-air region behind the base lowers the base pressure. A sketch of the phenomena is shown in figure 13(a). As  $p_0$  increases, the base-pressure ratio would be expected to decrease since the velocities of the turbulent oscillations are proportional to the velocity of the wake, which in this range of  $p_0$  is increasing with  $p_0$ . It will be noted that, for several values of  $p_0$  (for example,

40.7 inches of mercury), two observations are presented in figure 12 to show the unsteady character of the flow.

As  $p_0$  increases to a value for which the shock is first driven downstream of the base ( $p_0 \approx 60$  inches of mercury), the base-pressure ratio continues to decrease in the manner that has been described, but the rate of decrease is less, probably because the large vortices that dip deeply into the region behind the base tend to move downstream with increasing  $p_0$ . Once the flow is fully supersonic at  $M = 1.55$  ahead of the base, a strong oblique shock occurs at the corner of the base. When  $p_0$  exceeds about 60 inches of mercury, the wake boundaries appear to break down and cause the large vortices to move upstream toward the base again. These vortices seem to reach their greatest intensity just below  $p_0 \approx 80$ . In this region ( $p_0 \approx 60$  to  $p_0 \approx 80$ ) the base pressures of figures 8 and 11(a) show a distinct decrease. When  $p_0 = 80$ , the base pressure suddenly increases. The schlieren observations show that the large vortices are suddenly eliminated near this value of  $p_0$  and that the pattern of the flow reverts to that which exists at  $p_0 < 60$ . The latter would seem to indicate that, in this range of  $p_0$  (60 to 80), the breakdown of the wake boundaries into large and intense vortices close to the base is a severe transient condition rather than any back-pressure effects at the exit of the test section or effects from interaction of the wake and the reflected oblique shocks.

From a  $p_0$  of 80 to about 95, the base pressure again decreases slightly; this effect appears to be associated more with a weakening of the shock at the base edge to a strength which seems comparable to that for the lip shocks of supersonic base phenomena rather than with any appreciable expansion at the base. Between  $p_0 = 90$  and 95, the base pressure undergoes an abrupt decrease shown clearly by figures 8 and 11(a). In this range, the flow undergoes an expansion at the base corner, as indicated by the schlieren photographs. From  $p_0 \approx 95$  to 140, the expansion at the base increases until, at  $p_0 \approx 140$ , the base phenomena resemble those known to exist for two-dimensional bases in supersonic flow. The base pressure decreases accordingly.

The results presented in figure 10, with the center jet inactive and no splitter plate, show an orderly decrease of static pressure along the wall of the outer stream with increasing stagnation pressure up to a value of  $p_0 = 140$  where a fully supersonic flow is established.

With splitter plates.- From  $p_0 = 30$  to  $p_0 = 60$ , the base pressure with splitter plate is slightly higher than that for no splitter plate as shown in figures 8 and 11(a). An explanation for this difference is obtained by a comparison of the schlieren photographs of figures 12 to 15.

(See  $p_0 = 36.6$  and  $40.7$ , for example.) The splitter plate is seen to lessen the turbulent scavenging by preventing the formation of the large vortices and to damp the tendency of the vortices to dip deeply into the dead-air region. This effect is illustrated by a sketch in figure 13(b) which may be compared with the sketch of the phenomena with no splitter plate. (The dark streaks in some of the photographs are caused by oil collecting on the windows during the run or from previous runs.)

From  $p_0 = 60$  to  $p_0 = 80$ , the base-pressure variation with splitter plates shows none of the sudden decrease and subsequent increase which occurred without a splitter plate. Comparison of the schlieren photographs with and without splitter plates for this range of  $p_0$  shows that the breakdown of the wake boundaries into violent vortex action is completely eliminated by the presence of the splitter plate and that the flow continues its orderly transition toward a pattern common to a supersonic base.

From these results, the action of the splitter plates in appreciably increasing the base pressure approximately 30 percent in the stagnation-pressure range of 60 to 80 is clearly that of preventing the vortices shed by each base edge from forming into a common and large vortex street. Investigations in the high subsonic and transonic speed ranges of blunt trailing-edge airfoils, sheet-metal joints (the sheet-metal joint corresponds to a base with a splitter plate), and a two-dimensional flat plate normal to the stream in a water tunnel (see refs. 5 to 7) show increases in base pressure and corresponding decreases in base drag through the splitter-plate action in eliminating or appreciably suppressing the vorticity associated with the regular Karman vortex street. A somewhat similar action has been indicated to take place on a cylindrical body of revolution with the addition of a sting  $3/5$  of the base diameter in the transonic speed range as shown by reference 8. The flow conditions observed in the present investigation thus provide additional information on the drag reduction measured at the high subsonic and transonic speeds due to splitter-plate installation.

During the starting cycle, the static pressure at the lip of the base (obtained by orifice 9) is increased by the addition of a splitter plate as shown by figures 10 and 11(b). This effect is probably due to the action of the splitter plate in reducing the violent vortex action and, consequently, some of the induction effects at the lip which would normally be present in the absence of a splitter plate. These effects are, of course, reduced in progressing further upstream as shown by orifices 10 to 14 in figure 10.

Observations of tufts glued to the base plate and splitter plates gave an indication of the velocities and their directions along the surface of the base and splitter plate. Regardless of the value of  $p_0$ ,

the flow outward from the center of the base toward the base edges appeared to be rather steady. The velocity of this flow appeared to increase with  $p_0$ , this being most noticeable as the supersonic expansion about the base began.

The flow along the splitter plates was somewhat erratic at the very low values of  $p_0$ ; however, there did appear to be a consistent flow toward the base, particularly within two to three inches of the base. At the higher values of  $p_0$ , the direction of flow was well-defined and is indicated by the results shown in figure 16 which give the point of division between forward and reversed flow along the splitter plates as a function of  $p_0$ . These measurements may be considered accurate to  $1/8$  inch. The point of flow division moves rapidly toward the base as the expansion about the base increases. Beyond  $p_0 \approx 140$  the movement becomes small; this result agrees with the observed behavior of the base pressure and corresponds to the stable condition for supersonic base phenomena at  $M = 1.55$  ahead of the base.

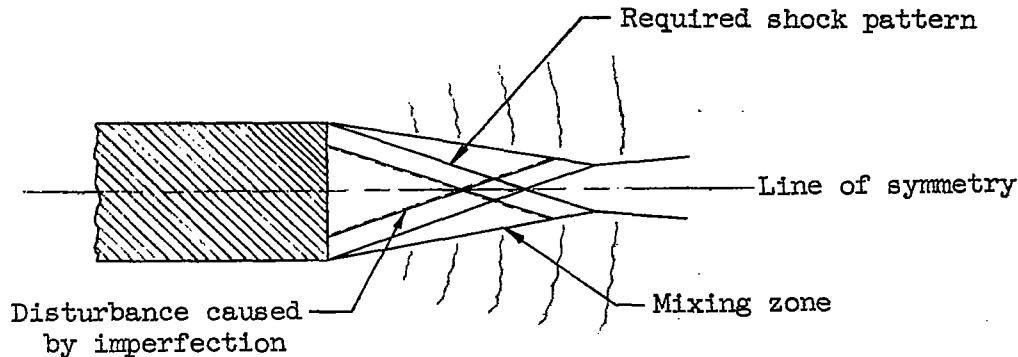
#### Fully Established Supersonic Flow

Outer streams only.- The flow over the base becomes fully supersonic at  $p_0 = 140$  as shown by the negligible variation of  $\frac{p}{p_0}$  beyond  $p_0 = 140$  in figure 8 and the convergence of the flow downstream of the base from both the upper and lower streams in the schlieren photographs of figure 12. This negligible variation of  $\frac{p}{p_0}$  is to be expected since a fully turbulent boundary layer existed ahead of the base for all values of  $p_0$ .

Increasing the splitter-plate thickness gives a slight increase in the base pressure as shown by the orifices in figure 8 or more clearly by orifice 4 in figure 11(a).

Center jet.- Results from tests involving the use of the center jet only are confined to schlieren photographs shown in figure 17. No base pressures are presented, since the pressures obtained by means of orifice 1 located on the lip of the base were approximately equal to 26.0 inches of mercury absolute regardless of the values of  $p_j$  when the flow from the center jet was supersonic. These photographs are included to make available a means for qualitative comparison with the flow of the center jet when the outer streams are operating. It will be noted in this figure that the schlieren photograph taken at  $p_j = 922$  (as an example) in the column labeled "vertical knife-edges" has some disturbances near the center of the jet which arise from points ahead

of the jet exit. These disturbances are caused by an imperfection in the machining of the center-jet nozzle. The sketch below will perhaps show their location more clearly.



These disturbances do not have sufficient strength to alter the flow patterns from the predicted patterns as will be shown in a later figure.

Center jet with outer streams. - The variation of the static pressures for the outer stream measured on the outer surface of the center-jet housing (see fig. 7) with both the center jet and outer streams operating simultaneously at different values of  $p_0$  is shown in figures 10 and 11(b). The values of  $\frac{p}{p_0}$  are not confined to any particular value of  $p_j$ . For the values of  $\frac{p}{p_0}$  shown, the stagnation pressures of the center jet were varied between 168.8 and 807.9 with several different values of  $p_0$  giving the same value of  $\frac{p}{p_0}$  at constant  $p_0$ .

The jet effect on the static pressures is seen by comparing the circle symbols with and without flags. The only significant variation occurs in the stagnation pressure range below  $p_0 = 65$  for the orifice located nearest to the lip of the base (orifice 9). The reduction in static pressure on the surface just ahead of the base caused by the center jet appears to be associated with the induction effects of the jet upon low energy air in the boundary layer, and the elimination of the large semi-dead air region downstream of the base by the presence of the jet. These flow conditions are illustrated in figure 18 which presents photographs of the outer streams at  $p_0 = 55$  with and without the center jet.

A series of double-image schlieren photographs of the phenomena associated with the interaction of the outer streams and center jet is

shown in figure 19 for a condition of constant outer-stream stagnation pressure and variable center-jet stagnation pressure. The value of  $p_o = 61.1$  was taken as an illustrative example of the flow conditions at the lip. At this outer-stream stagnation pressure, the flow has just become supersonic (at the lip) when there was no center-jet flow. (See fig. 12.) Comparison of figures 12 and 19 shows that the center jet has no apparent effect on the flow pattern in the outer stream ahead of the base lip when  $p_o \approx 65$  or greater, and this result is in agreement with the variation of the static pressures mentioned in the preceding paragraph. When photographs from figures 17 to 20 with and without the outer stream and at various combinations of stagnation pressures for both the center jet and outer streams are compared, the mutual effects of one flow on another in increasing the downstream extent of supersonic flow are apparent.

Predictions of flow field.- Enlargements of schlieren photographs of the flow over the base for different values of  $p_o$  and  $p_j$  are shown in figure 21 with the theoretical shock patterns and boundaries or mixing zones superimposed on the actual patterns. The patterns in figure 21 were selected as illustrative examples since they best represent typical flow patterns obtained in the mixing-zone apparatus for the range of  $p_o$  and  $p_j$  values investigated. The predictions of the various shock waves and mixing zones were obtained by use of the regular shock equations, equations of the Prandtl-Meyer expansion around a corner (found in refs. 11 and 12, respectively), and two-dimensional characteristics.

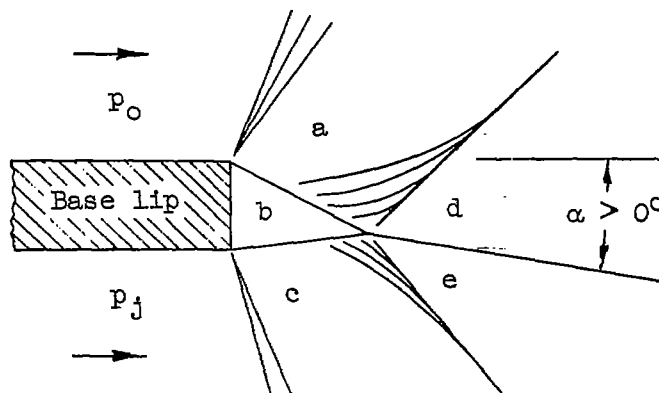
The prediction of the flow field downstream of the base with the center jet only, shown in part (a) of figure 21, gives very good agreement with the actual flow field. This agreement shows that the disturbances caused by poor machining of the center-jet nozzle have very little, if any, effect on the jet field.

For the prediction of the flow field downstream of the base with both the center jet and outer streams operating simultaneously, shown in parts (b) to (f) of figure 21, the base lip between the two supersonic streams was assumed to have zero height. (Actually, the height was 1/16 inch as shown in fig. 7.) The first step is to determine the turning of the mixing zone between the two supersonic streams. This can be accomplished by obtaining a pressure equivalence across the mixing zone through a trial-and-error manipulation of the shock and expansion equations. Once the turning angle of the mixing zone is established, the shock angles within the center jet are easily determined. (An explanation as to the determination of the flow boundaries at the base lip, shown in fig. 21, is discussed in connection with the base-pressure prediction.)

When the shock which appears to pass through the mixing zone shown in parts (c), (e), and (f) of figure 21 is determined, a trial-and-error method must again be used for obtaining the static-pressure equivalence across the mixing zone downstream of the shock. It should be emphasized that the mixing zone between the outer stream and the center jet is supersonic. Thus, in effect, the shock actually passes through the mixing zone and unites with the shock caused by the turning of the mixing zone in the outer stream. It is obvious that the mixing zone downstream of the shock juncture must turn through an angle that would allow the flow in the center jet to remain parallel to the axis of symmetry or else to expand initially to some small angle and then gradually turn parallel to the axis of symmetry. For the examples shown in figure 21, the theoretical mixing zone diverges initially approximately  $1^\circ$  to  $1.5^\circ$  from the axis of symmetry. The expansions caused by this divergence reflect from the axis of symmetry and pass through the supersonic mixing zone and thus cause the zone to turn parallel to the axis. Additional schlieren photographs illustrating this effect may be found in reference 13. The prediction of the continuous shock passing through the mixing zone is very good if the initial assumption and exclusion of viscous effects are considered. It should be emphasized that the calculations for the flow field are not essential for the prediction of the base pressure.

#### Base Pressure Between Center Jet and Outer Streams

For a better understanding of the procedure used in predicting the base-pressure coefficient by means of the semiempirical method presented in reference 4, a sketch of the manner in which the flow passes over the base separating two supersonic streams of different Mach numbers, stagnation pressures, and static pressures is shown as follows:



It is seen from the sketch that the flow over the base lip is similar to that of flow over a two-dimensional base, where the body is at an angle of attack  $\alpha$ . The angle of the mixing zone  $\alpha$  is determined by the method presented in connection with figure 21 for obtaining static-pressure equivalence in regions d and e of the sketch. The angles of the boundaries between regions a and b and between regions b and c are determined by the semiempirical method presented in reference 4. As was mentioned previously, this method makes use of the analogy established between the flow about a two-dimensional base and the pressure rise required to separate the boundary layer. The separation of the boundary layer is accompanied by an angular change in flow direction and it is assumed that the angles of change in flow direction are equal to the turning angles of the boundary of regions a and d and the boundary of regions c and e as a function of the Mach numbers in a and c, respectively. These angles are presented in reference 4 as functions of the calculated Mach numbers upstream of the base lip. A total effective turning of the flow in region a is then obtained by adding the angle of attack of the body, the angle of the boundary of regions a and d, and the angle of turning required to obtain the Mach number in the region designated by  $p_0$ . From this sum, the Mach number and pressure are obtained in region a. A similar procedure is used to obtain the Mach number and pressure in region c with the exception that the angle of attack of the body is subtracted. The average of the static pressures in regions a and c is then assumed to be the pressure on the base between the outer stream and the center jet. The above procedure was used in the calculation of the base pressure for the present investigation and is represented by the solid curve in figure 22. The dashed curve is calculated by the same procedure but is based upon the empirical refinement to the variation of the pressure-rise coefficient with Mach number given in reference 4.

The base-pressure coefficient may also be predicted through a trial-and-error manipulation of the shock-expansion equations by varying the turning angle of the mixing zone  $\alpha$  such as to obtain equal pressures in regions a and c. The sum of the turning angles between regions a and d and regions c and e, obtained from reference 4, is assumed to be constant. It was found that the angle of the mixing zone  $\alpha$  obtained by the second method does not agree with the experimental angle as well as that calculated by the first method; however, the base pressure predicted by this second method agrees with the first within approximately 1 percent.

The calculations of the base pressures made in connection with this investigation were confined to an under-pressure jet; however, it is quite evident that they can be applied to an over-pressure jet as well.

It is seen from figure 22 that the prediction of the base-pressure coefficient gives good agreement with the experimental results.

The experimental results represent a variation of both the center jet and outer stream pressures and cover a range of pressure ratios involving 37 values of outer-stream stagnation pressure. A few of the experimental base-pressure coefficients shown represent check runs. Provided the flow of the outer stream and center jet is supersonic at the base lip, there is little effect of magnitude of outer-stream and center-jet pressures on the base-pressure coefficient at any particular value of  $\frac{P_2}{P_1}$ .

This result is to be expected since it is known that Reynolds number has little effect on the base pressure provided the boundary layer is turbulent. Schlieren photographs showing examples of the flow patterns at varying  $p_0$  and  $p_j$  values but at constant ratios of  $\frac{P_2}{P_1}$  are presented in figure 23. It is seen that the flow patterns are identical in the vicinity of the base for constant values of  $\frac{P_2}{P_1}$ .

The experimental base pressure above values of  $\frac{P_2}{P_1}$  equal to 0.75 are somewhat higher than the trend established by the base-pressure predictions and by the experimental results in the lower range of  $\frac{P_2}{P_1}$ .

(See fig. 22.) This result may be attributed to the pressures not settling out in the multiple-tube mercury manometer at the higher stagnation pressures as a result of the short running times. On the basis of these results, it appears that the method of reference 4 will give a good prediction of the pressure on a two-dimensional base separating supersonic streams of different Mach numbers, stagnation pressures, and static pressures.

Emphasis should again be placed on the fact that the method of reference 4 for predicting base pressure is restricted to flow having turbulent boundary layers upstream of the base as is the case of flow in the mixing-zone apparatus.

#### CONCLUDING REMARKS

An investigation has been conducted in a mixing-zone apparatus to determine the effects of jet flow on two-dimensional base pressure and of the development of supersonic channel flow about a two-dimensional base with and without splitter plates of different thicknesses. With fully developed supersonic flow, the Mach number of the outer streams ahead of the base was 1.55. For the center jet, the Mach number was 3.36. The results show that a good prediction of two-dimensional base pressure was obtained by use of the semiempirical method presented in NACA RM L53C02.

The flow pattern downstream of the base with both the outer streams and center jet operating simultaneously and both fully supersonic was predicted satisfactorily by use of the regular shock equations, equations of the Prandtl-Meyer expansion, and two-dimensional characteristics, provided the mixing zone was supersonic. Within the limits of this investigation, the base-pressure coefficient was unchanged when the absolute magnitudes of the center-jet and outer-stream pressures were varied provided the ratio of the two pressures remains constant. With use of the outer streams only and the center jet acting as a two-dimensional base, there was little or no variation of the base pressure across the base for any given value of outer-stream stagnation pressure. During the starting cycle, the base pressure was increased as much as 30 percent by the addition of the splitter plate; whereas for a fully developed supersonic flow the increase was very small. The effect of the splitter plate was to lessen the turbulent scavenging and thus increase the base pressure by preventing the formation of the large vortices of the Kármán vortex street.

Langley Aeronautical Laboratory,  
National Advisory Committee for Aeronautics,  
Langley Field, Va., February 19, 1954.

## REFERENCES

1. Cortright, Edgar M., Jr., and Kochendorfer, Fred D.: Jet Effects on Flow Over Afterbodies in Supersonic Stream. NACA RM E53E25, 1953.
2. Chapman, Dean R.: An Analysis of Base Pressure at Supersonic Velocities and Comparison With Experiment. NACA Rep. 1051, 1951. (Supersedes NACA TN 2137.)
3. Cortright, Edgar M., Jr., and Schroeder, Albert H.: Investigation at Mach Number 1.91 of Side and Base Pressure Distribution Over Conical Boattails Without and With Jet Flow Issuing From Base. NACA RM E51F26, 1951.
4. Love, Eugene S.: The Base Pressure at Supersonic Speeds on Two-Dimensional Airfoils and Bodies of Revolution (With and Without Fins) Having Turbulent Boundary Layers. NACA RM L53C02, 1953.
5. Hoerner, Sighard F.: Base Drag and Thick Trailing Edges. Jour. Aero. Sci., vol. 17, no. 10, Oct. 1950, pp. 622 - 628.
6. Hoerner, Sighard F.: Verschiedene Messungen (Various Measurements). Fieseler Water Tunnel, Rep. No. 2, 1939.
7. Summers, James L., and Page, William A.: Lift and Moment Characteristics at Subsonic Mach Numbers of Four 10-Percent-Thick Airfoil Sections of Varying Trailing-Edge Thickness. NACA RM A50J09, 1950.
8. Hart, Roger G.: Effects of Stabilizing Fins and a Rear-Support Sting on the Base Pressures of a Body of Revolution in Free Flight at Mach Numbers From 0.7 to 1.3. NACA RM L52E06, 1952.
9. Barry, Frank W., and Edelman, Gilbert M.: An Improved Schlieren Apparatus. Jour. Aero. Sci., vol. 15, no. 6, June 1948, pp. 364-365.
10. Burgess, Warren C., Jr., and Seashore, Ferris L.: Criteria for Condensation-Free Flow in Supersonic Tunnels. NACA TN 2518, 1951.
11. Neice, Mary M.: Tables and Charts of Flow Parameters Across Oblique Shocks. NACA TN 1673, 1948.
12. The Staff of the Ames 1- by 3-Foot Supersonic Wind-Tunnel Section: Notes and Tables for Use in the Analysis of Supersonic Flow. NACA TN 1428, 1947.
13. Wilder, John G., Jr.: Part I of Final Report on Phase I of the Study of Air Exchange Problems in Supersonic Tunnels. Rep. no. AD-570-A-5 (Contract No. W33-038 ac-21809), Cornell Aero. Lab., Inc., Jan. 1949.

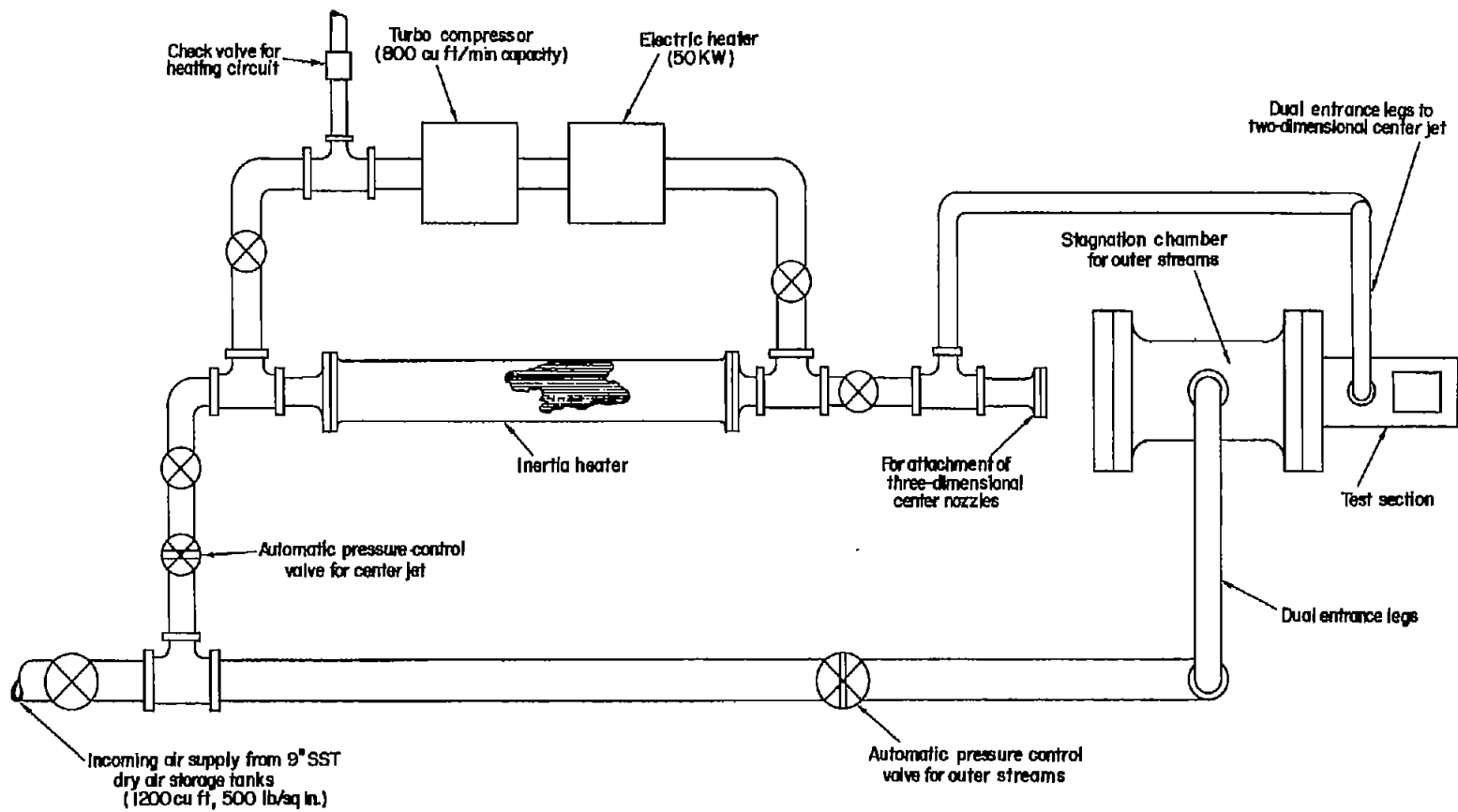


Figure 1.- Schematic drawing of the supersonic mixing-zone apparatus.

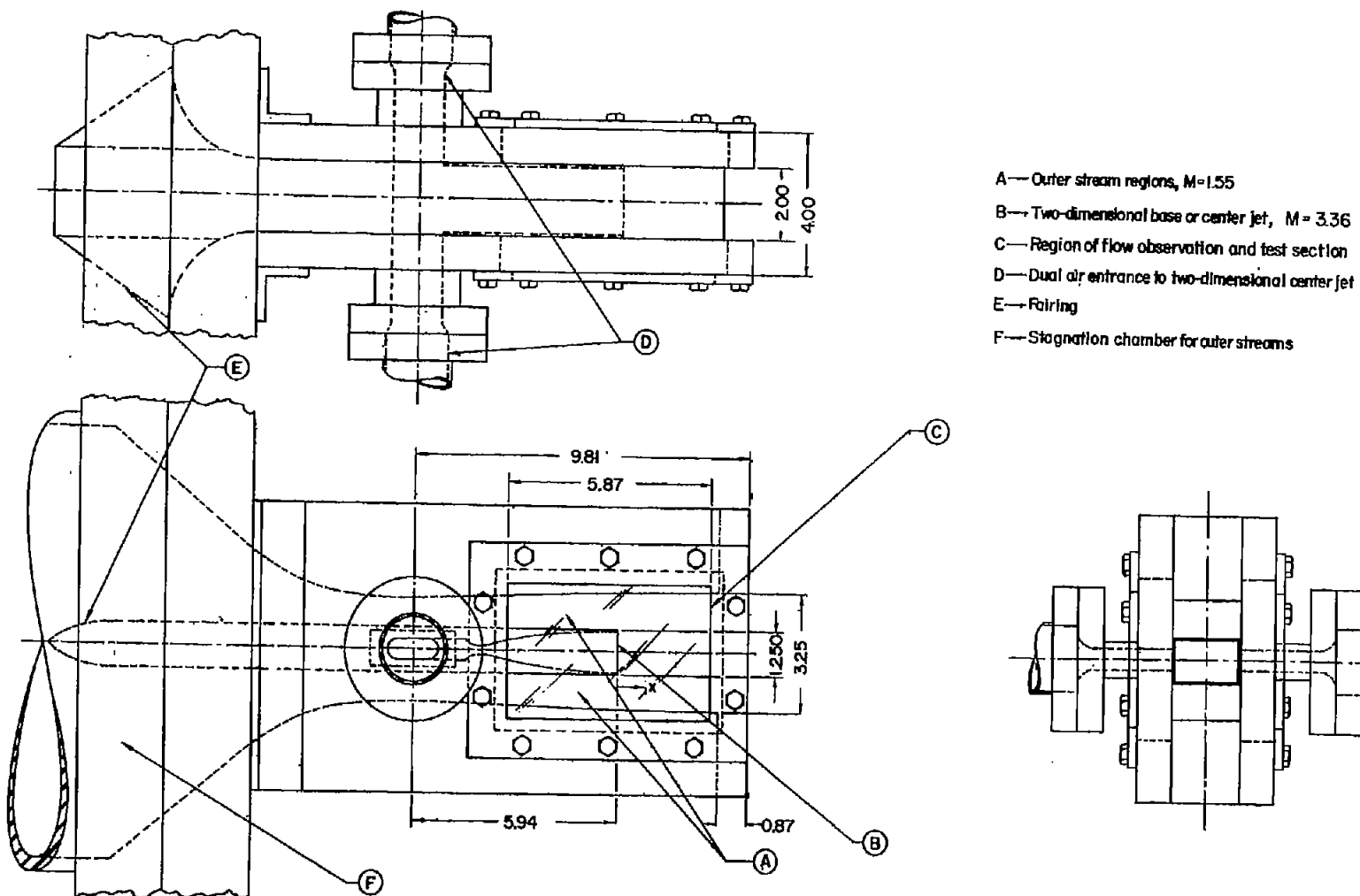
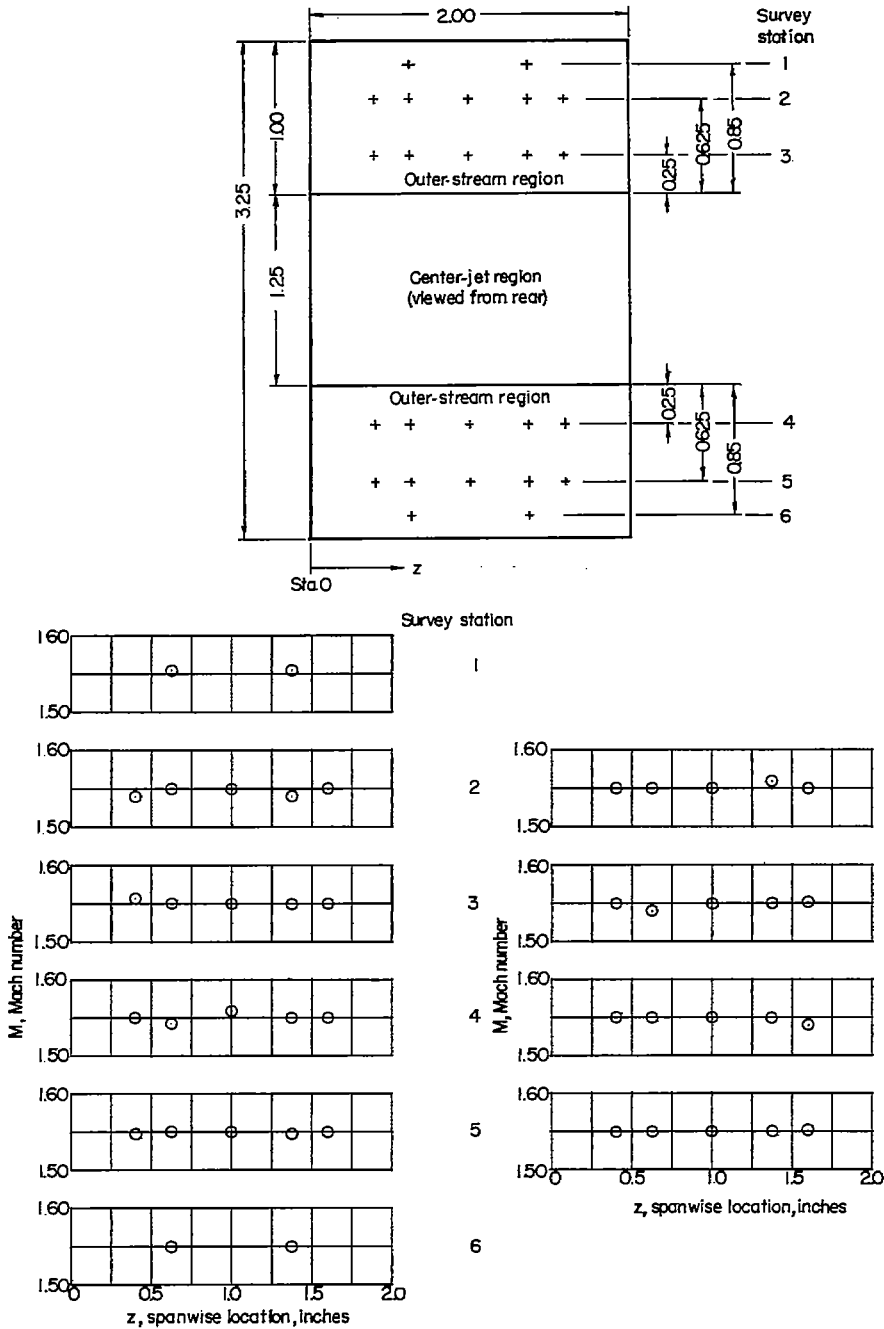


Figure 2.- Test section of the supersonic mixing-zone apparatus. All dimensions are in inches.



(a) Survey plane at  $x = 0$  inch.      (b) Survey plane at  $x = -0.5$  inch.

Figure 3.- Variation of Mach number in the outer streams at  $p_0 = 215.8$  inches of mercury absolute. (Same results obtained at  $p_0 = 83.5$  and  $142.5$  inches of mercury absolute.) All dimensions are in inches.

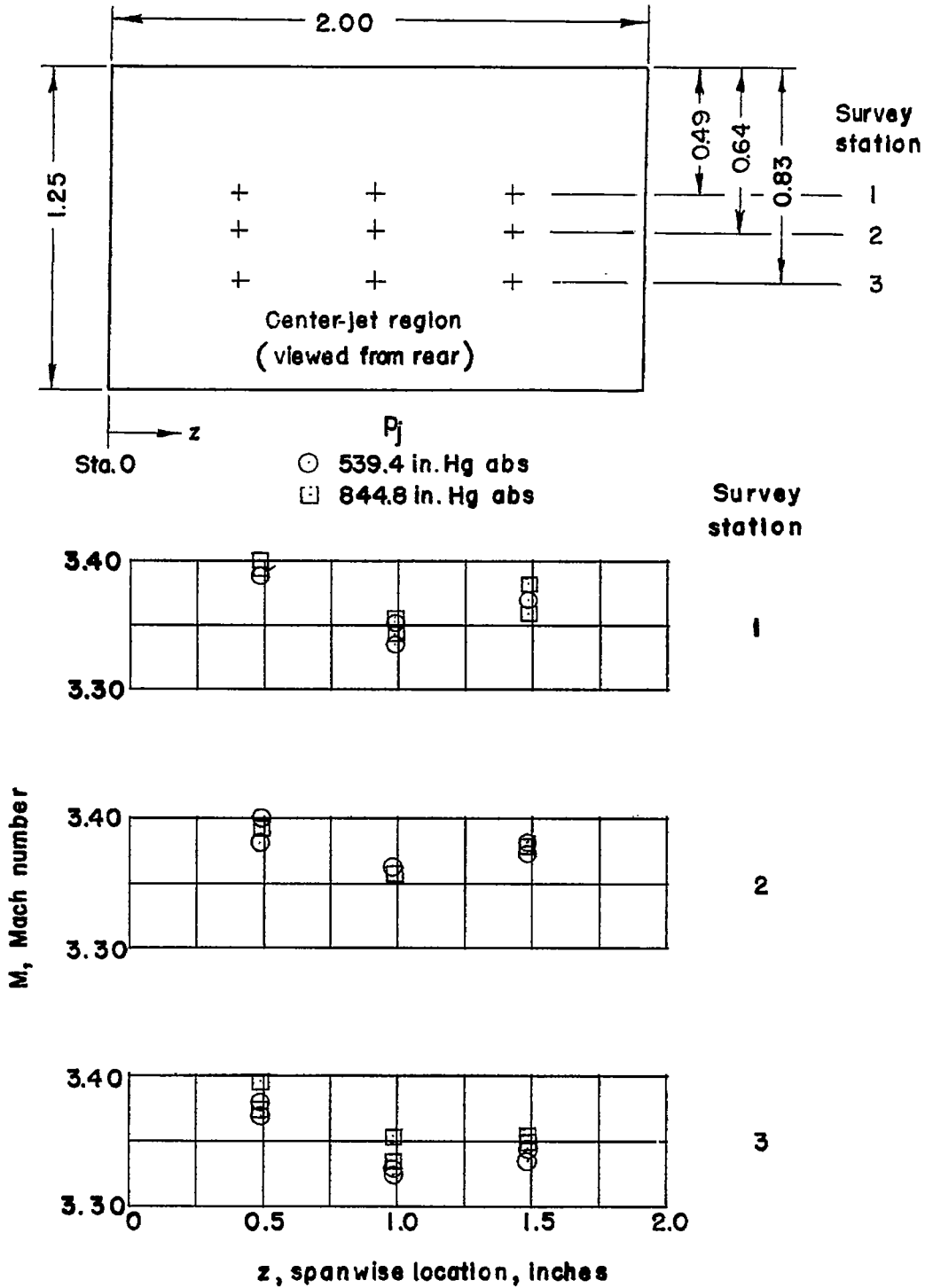
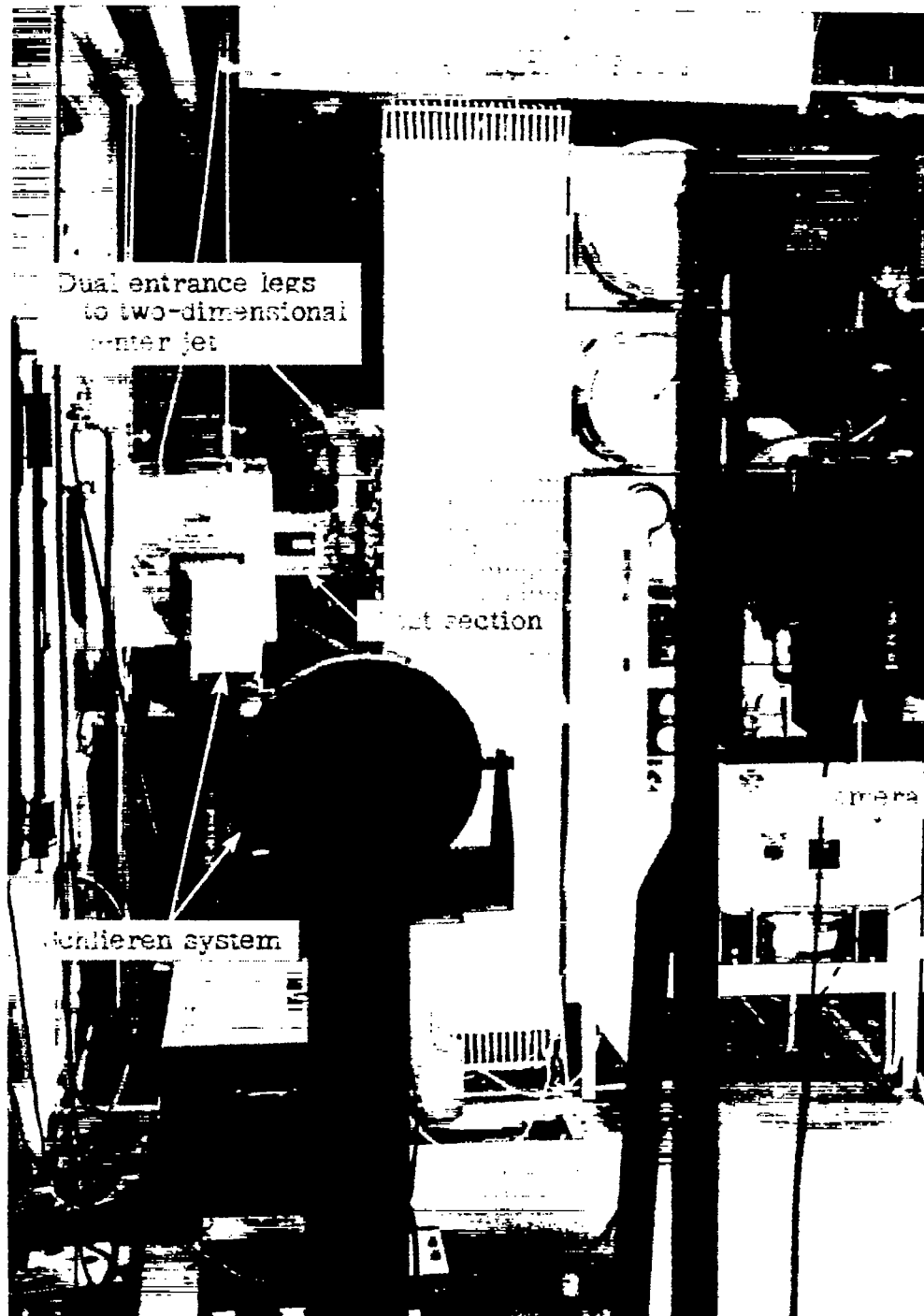


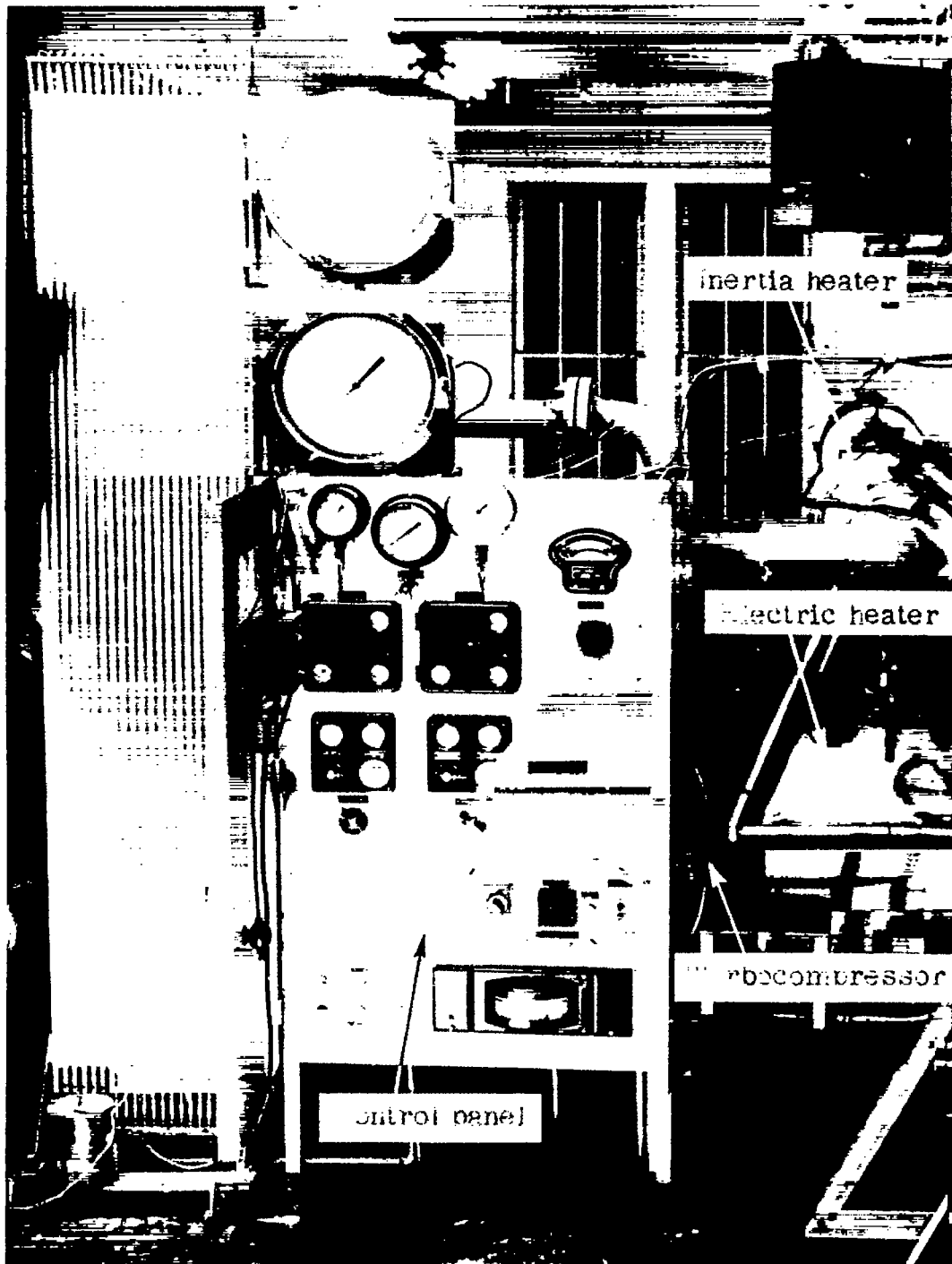
Figure 4.- Variation of Mach number in the center jet at  $x = 0$  inch survey plane. All dimensions are in inches.



L-78031.1

(a) View showing test section and schlieren system.

Figure 5.- Photograph of the supersonic mixing-zone apparatus setup.



L-78032.1

(b) View showing the control panel, heaters, and compressor.

Figure 5.- Concluded.



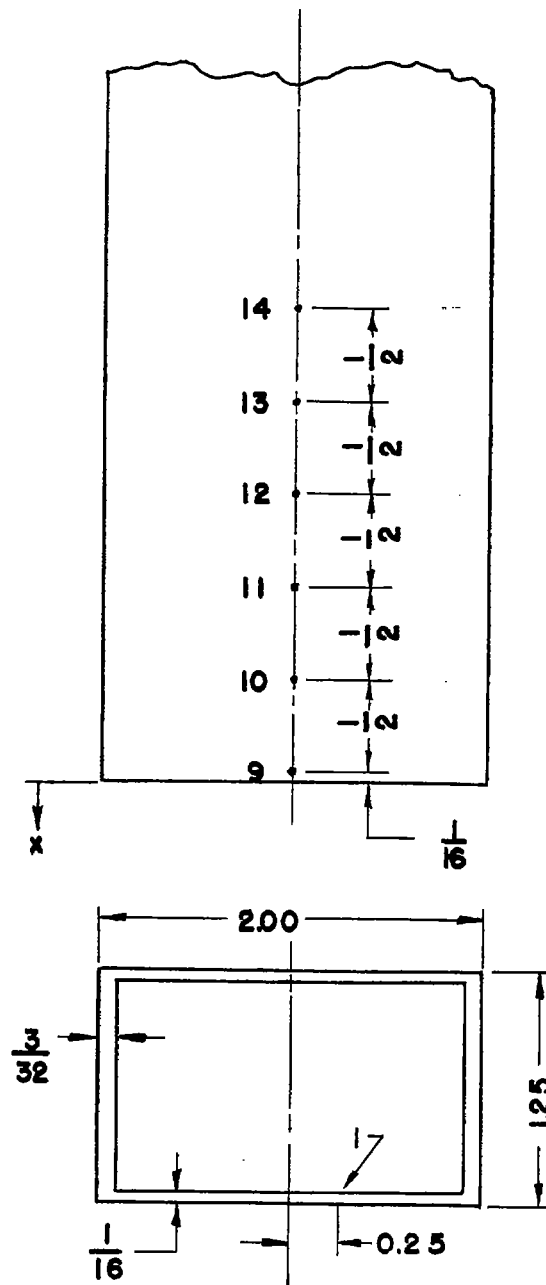
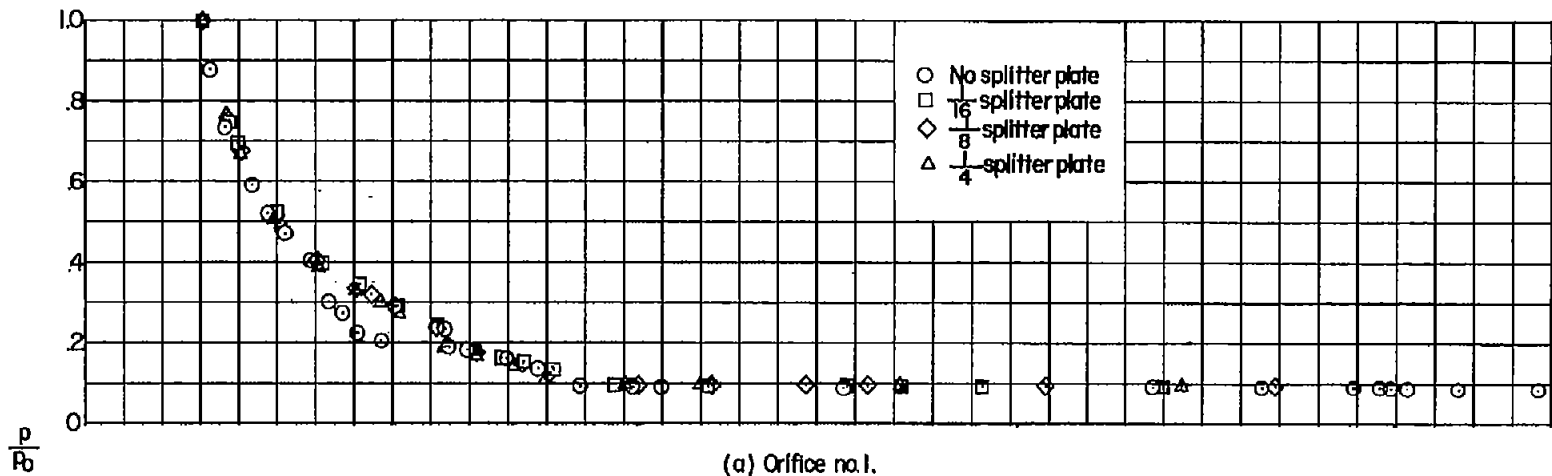
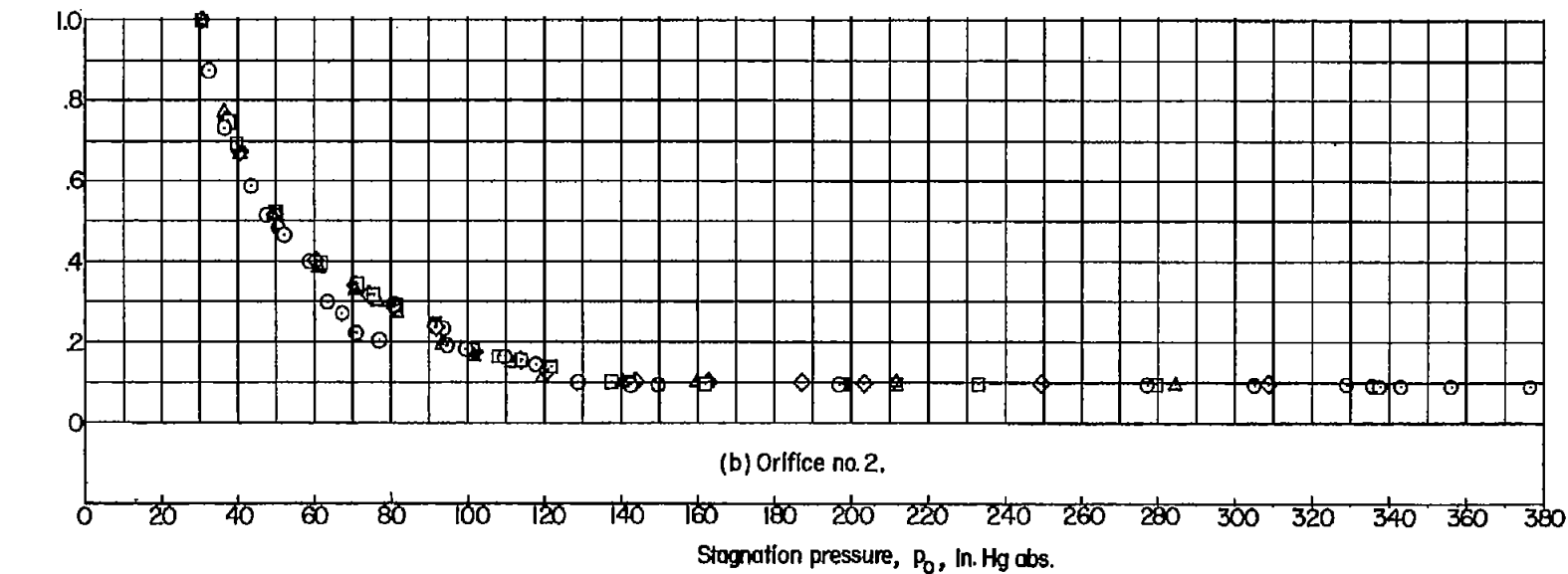


Figure 7.- Sketch of the static-pressure orifice location on the outer surface of the center jet housing. All dimensions are in inches.

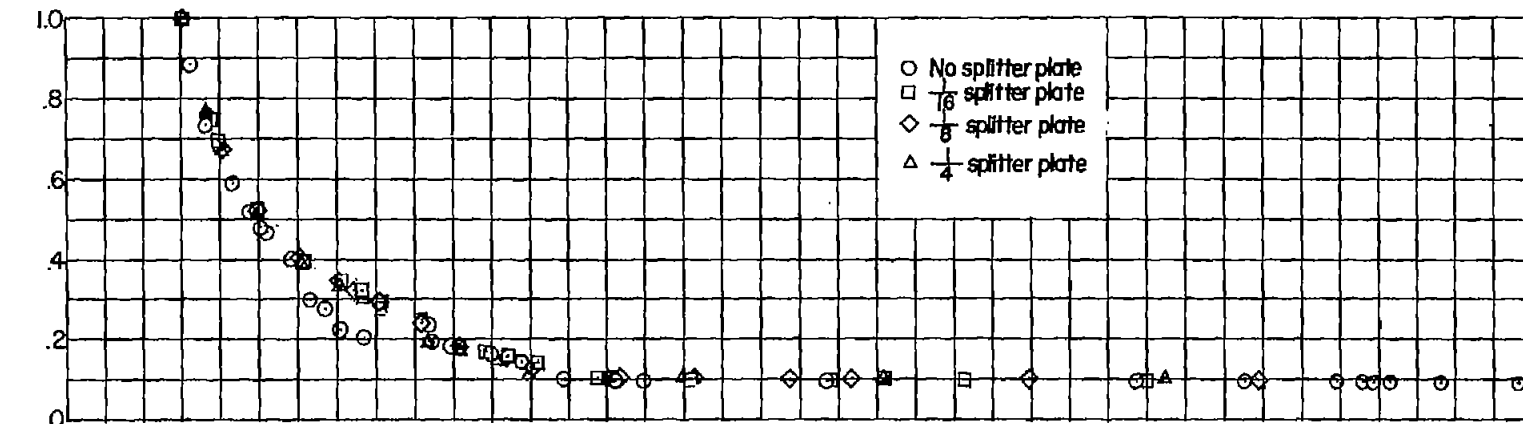


(a) Orifice no. 1.

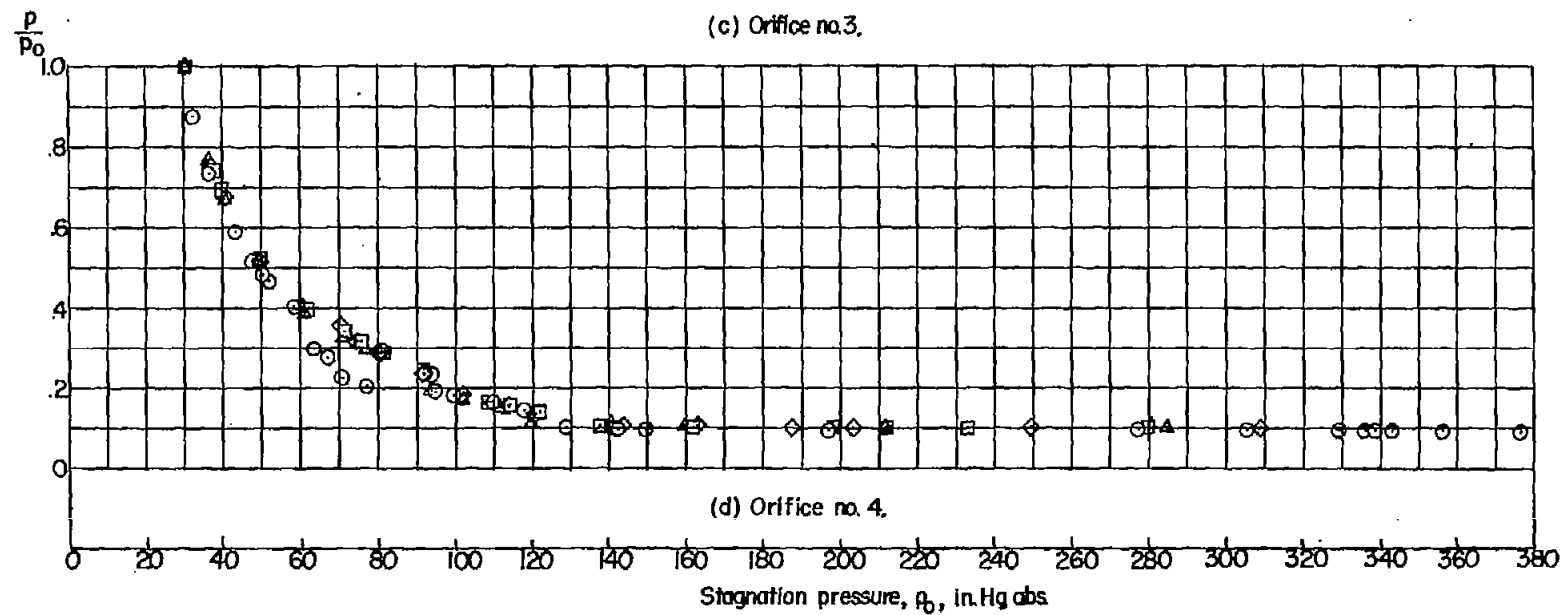


(b) Orifice no. 2.

Figure 8.- Variation of the ratio of base pressure to outer-stream stagnation pressure as a function of outer-stream stagnation pressure, with and without splitter plate or base plate.

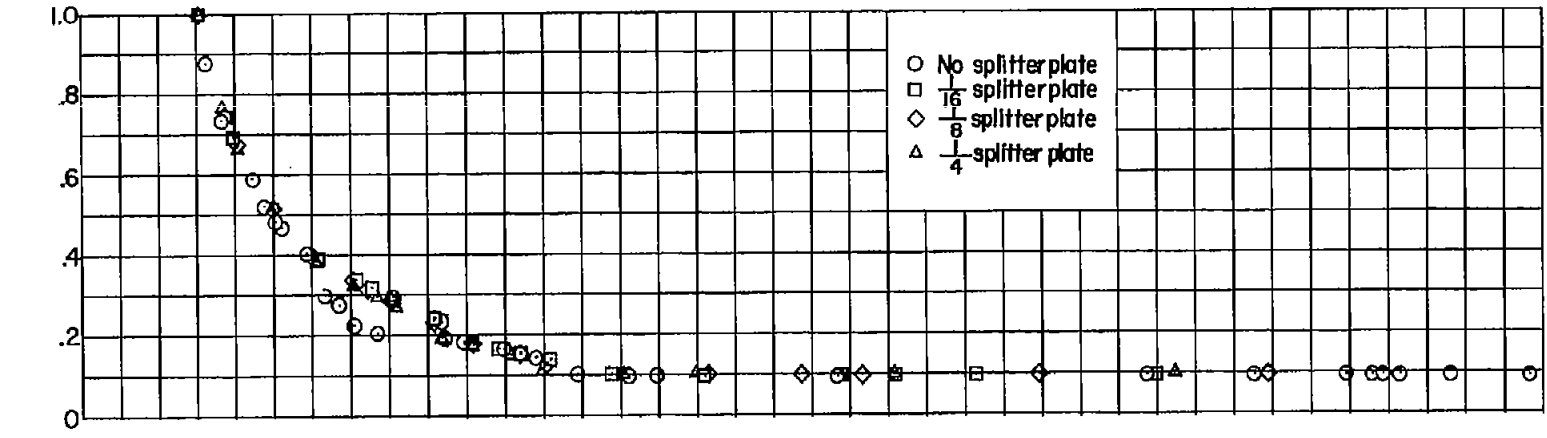


(c) Orifice no. 3.

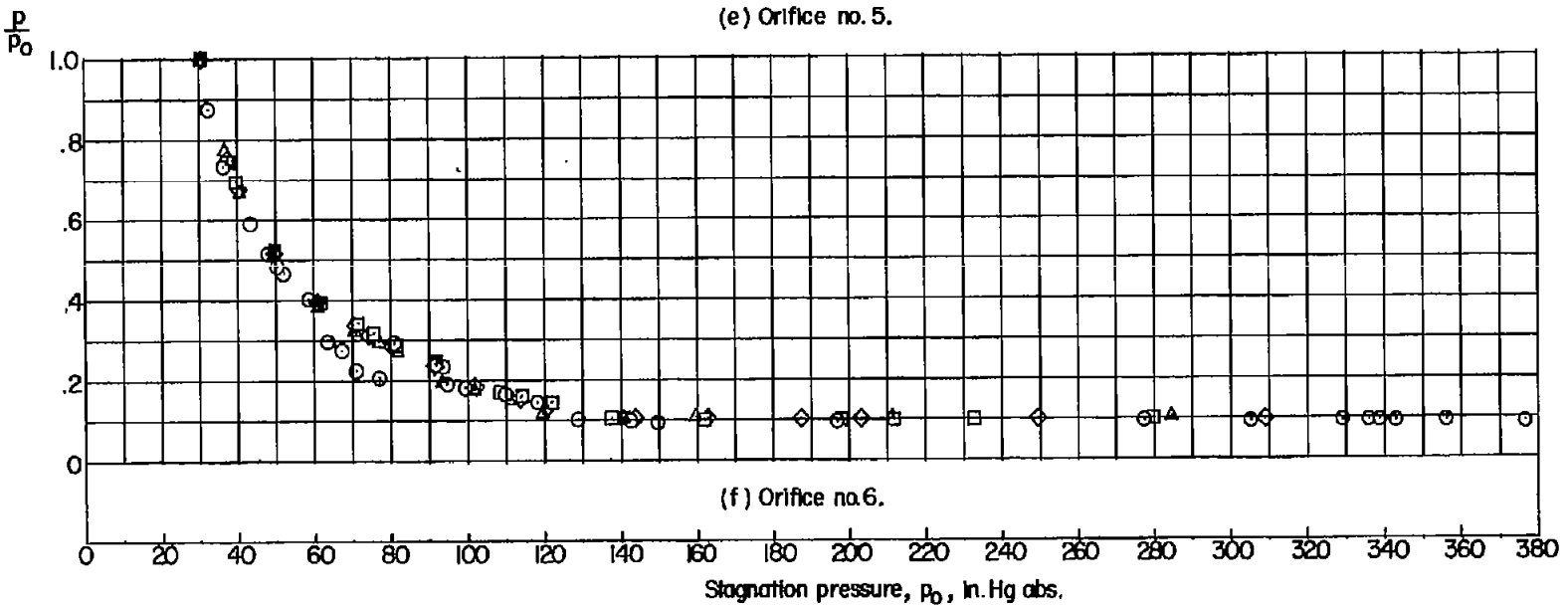


(d) Orifice no. 4.

Figure 8.- Continued.



(e) Orifice no. 5.



(f) Orifice no. 6.

Stagnation pressure,  $p_0$ , in. Hg abs.

Figure 8.- Continued.

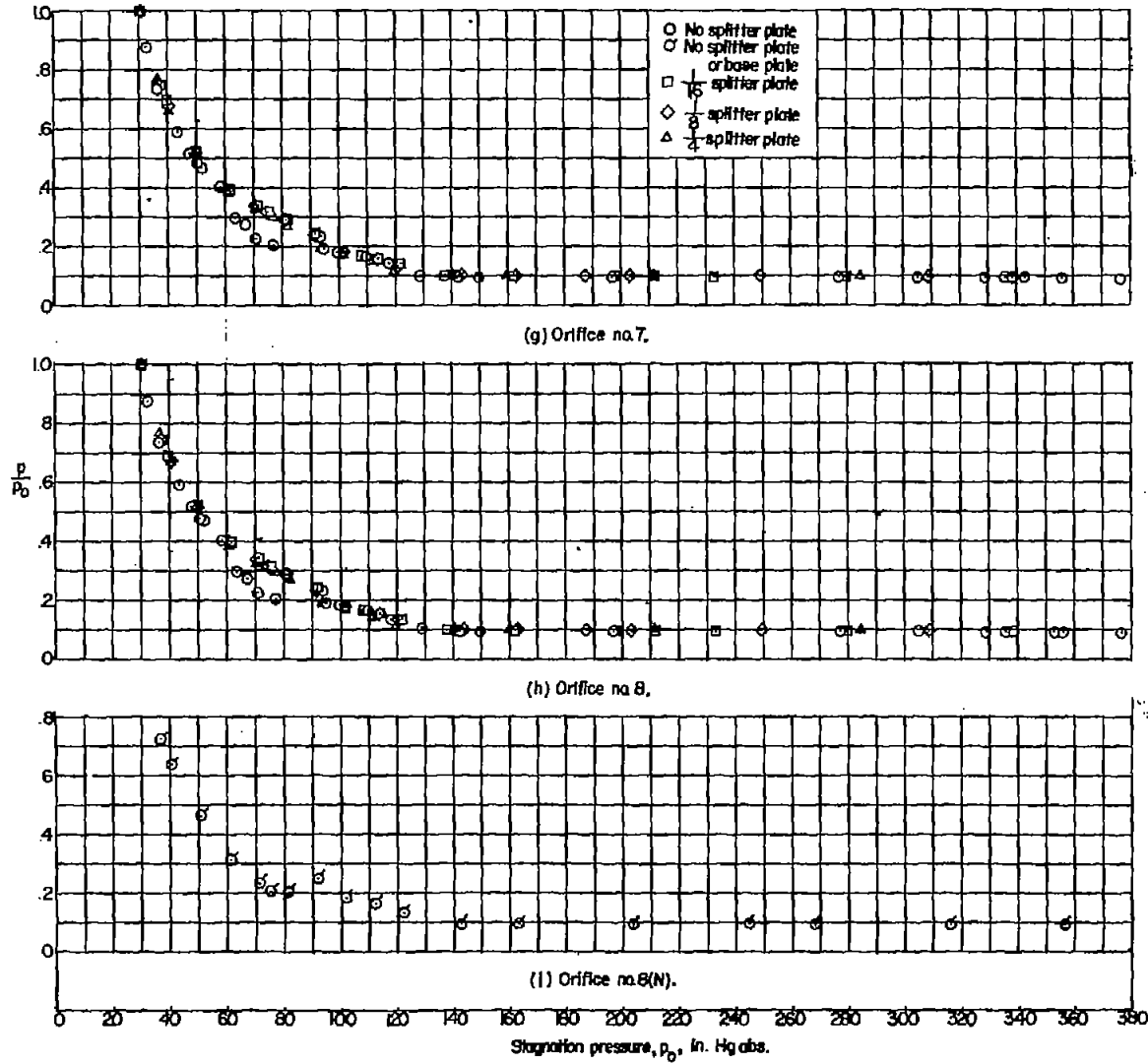
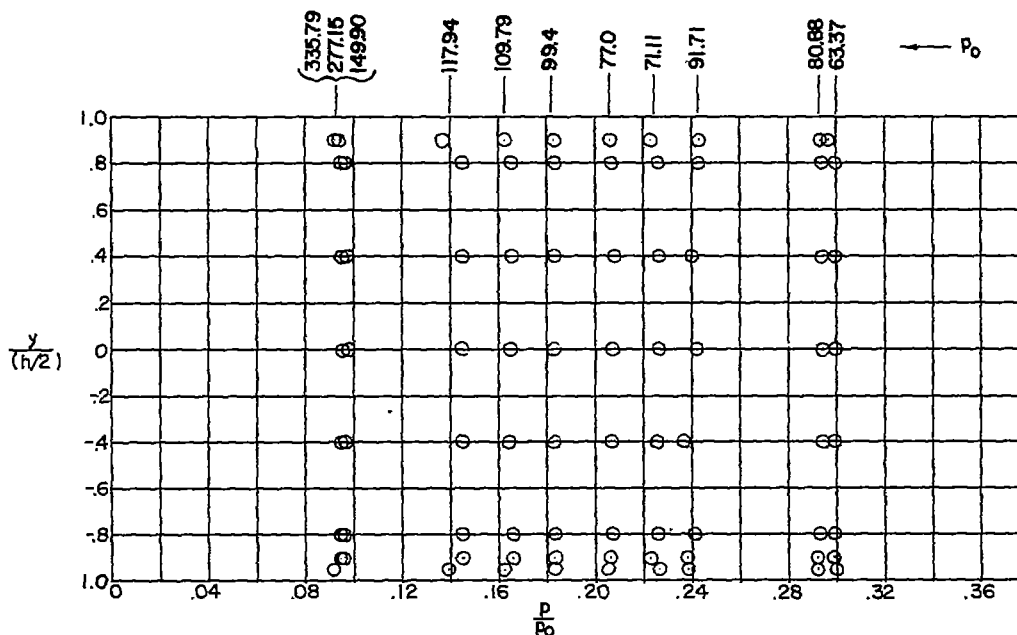
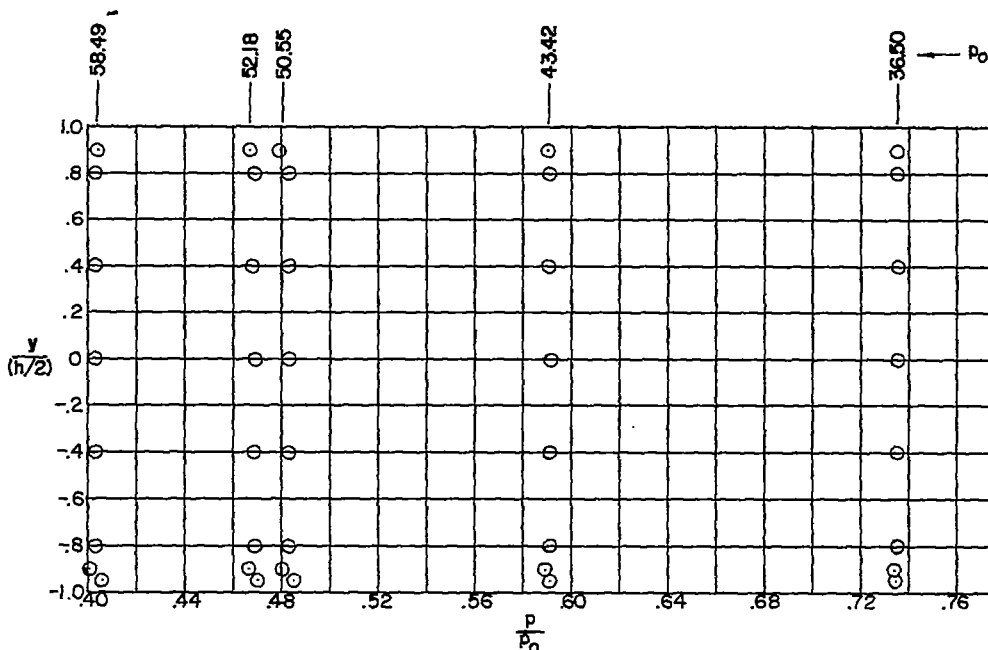


Figure 8.- Concluded.



(a)  $p_0$  values from 63.67 inches of mercury absolute to 335.79 inches of mercury absolute.



(b)  $p_0$  values from 36.50 inches of mercury absolute to 58.49 inches of mercury absolute.

Figure 9.- Pressure variation across the base plate (no splitter-plate) for different values of stagnation pressure.

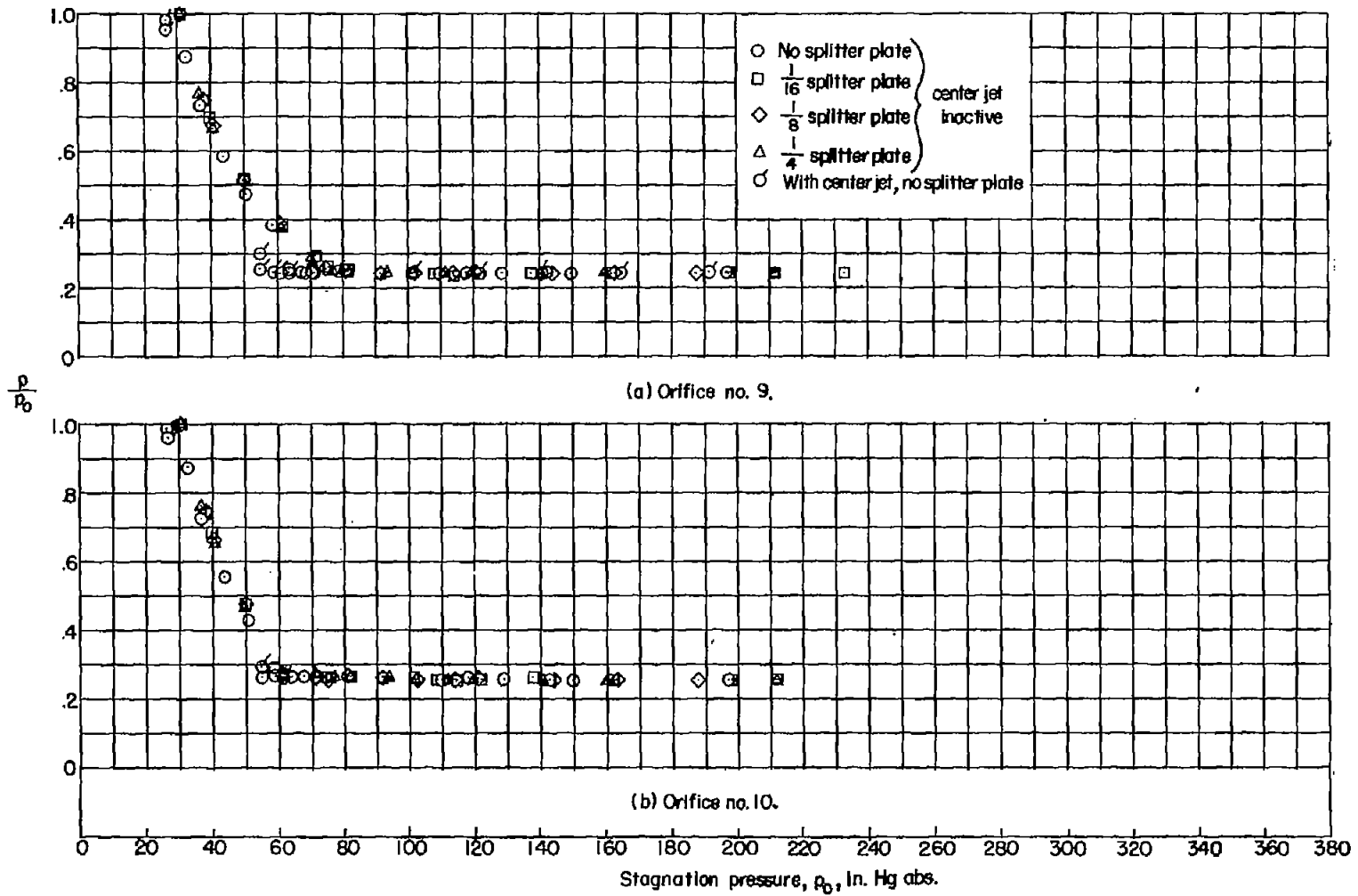
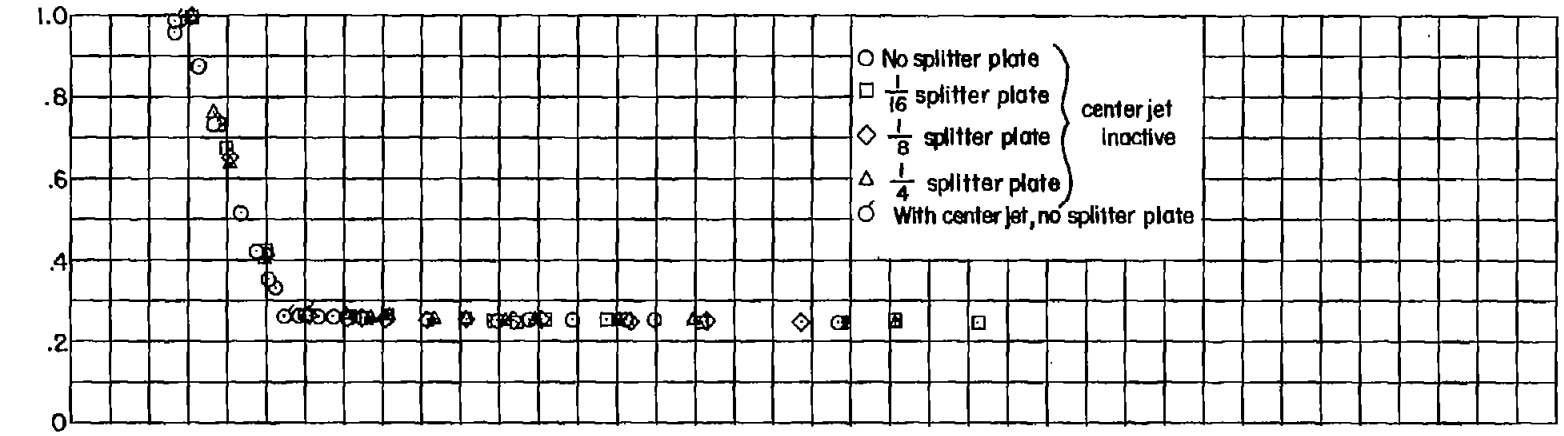
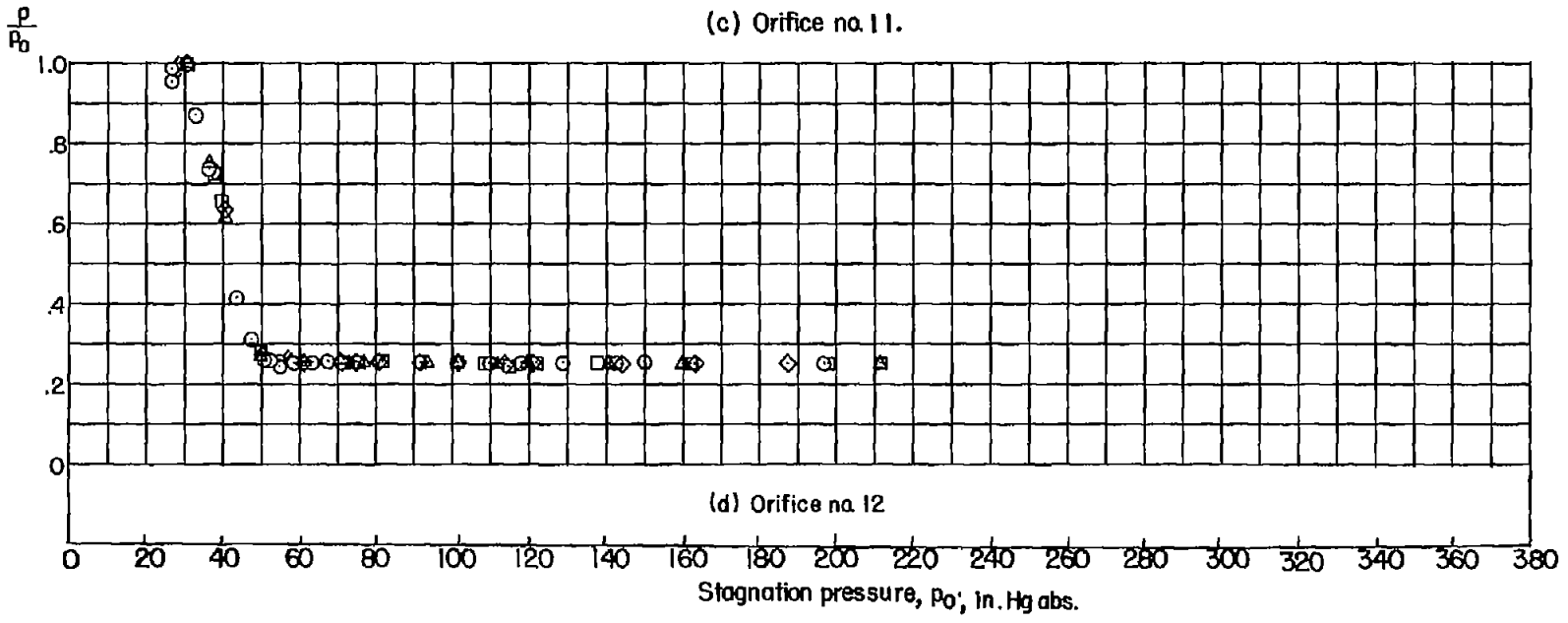


Figure 10.- Variation of the ratio of static pressure to outer-stream stagnation pressure for the outer stream as a function of the outer-stream stagnation pressure, with and without splitter plate or center jet in operation.



(c) Orifice no. 11.



(d) Orifice no. 12

Figure 10.- Continued.

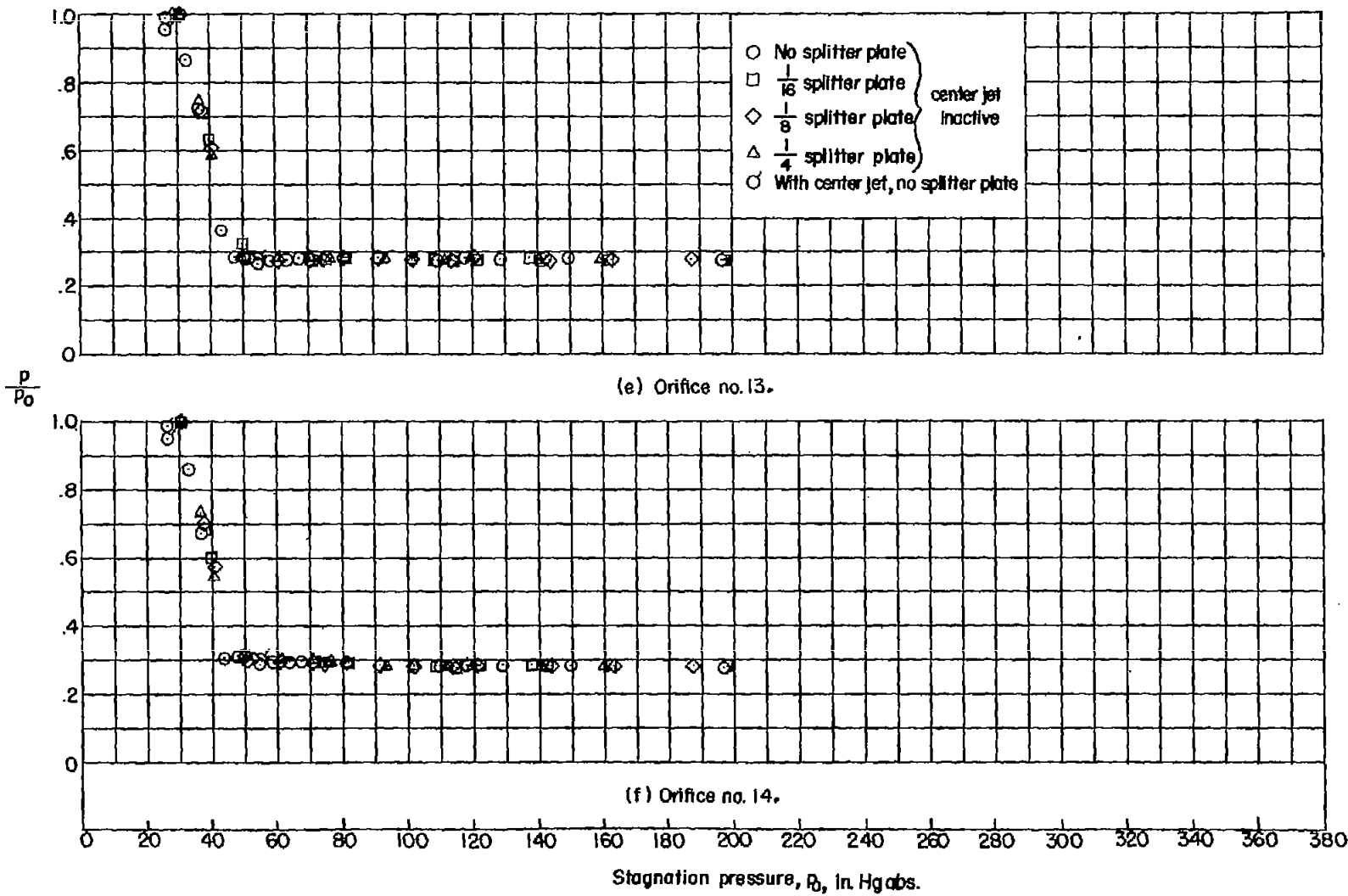


Figure 10.- Concluded.

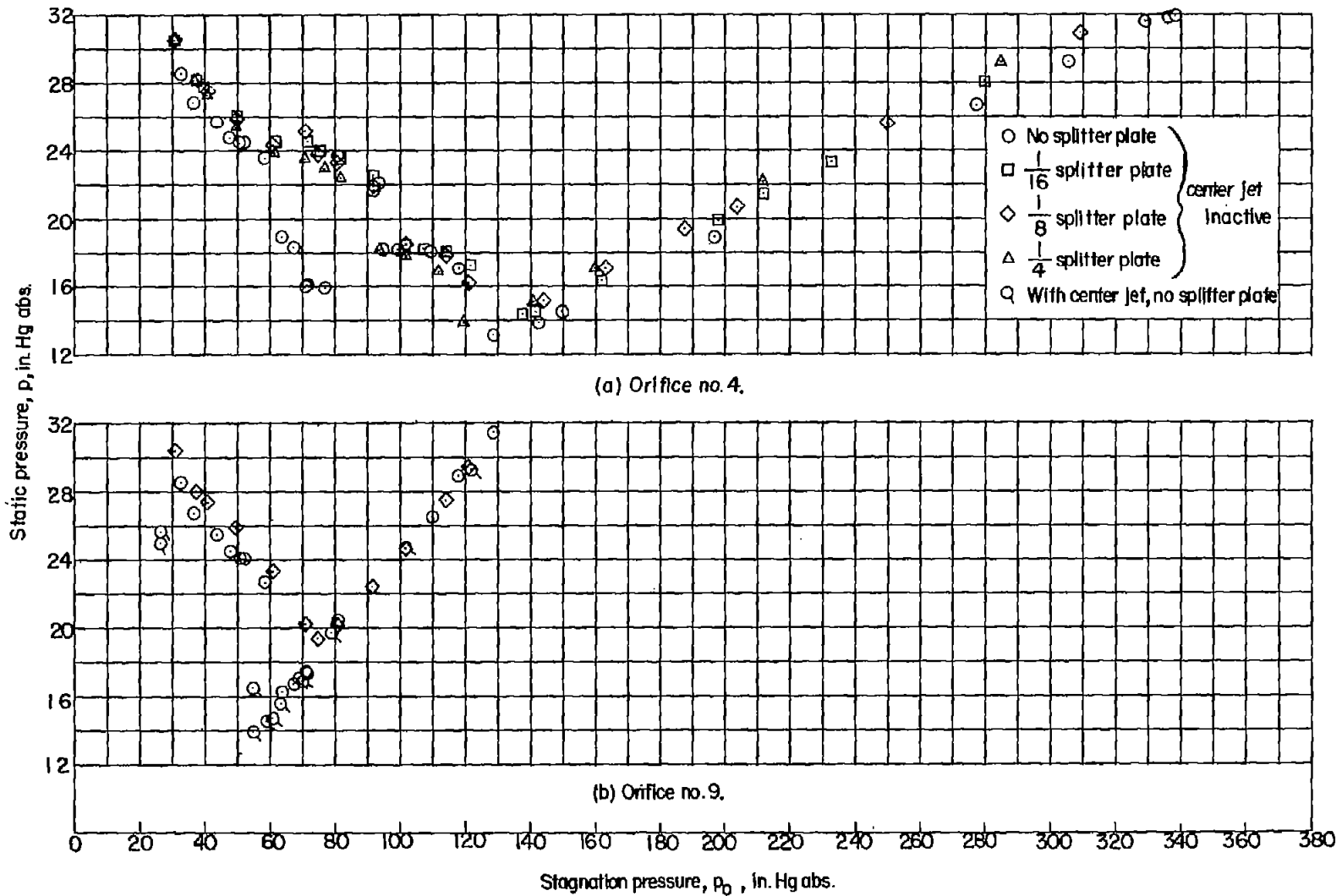


Figure 11.- Variation of the absolute static pressure as a function of the outer-stream stagnation pressure for two representative orifices.

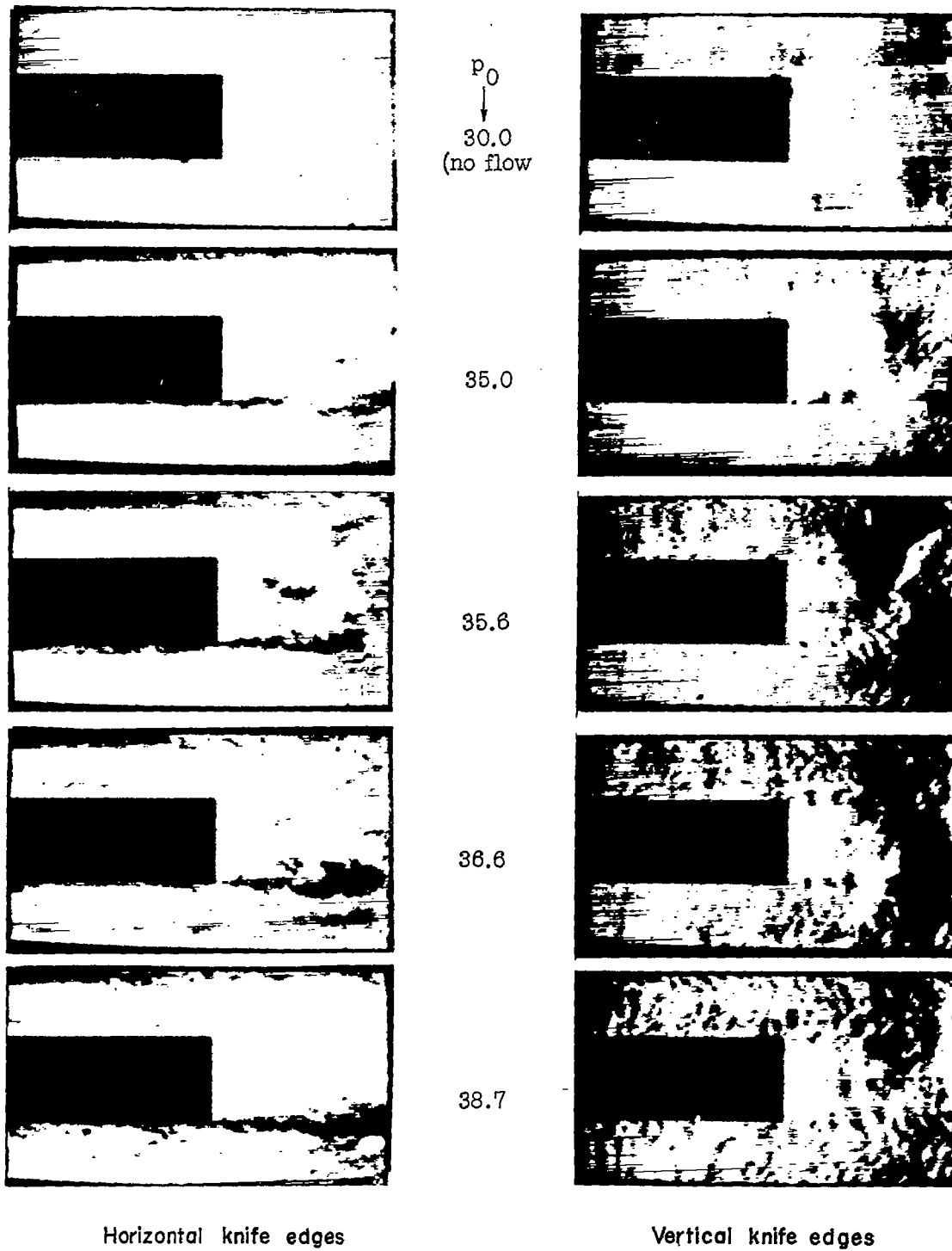
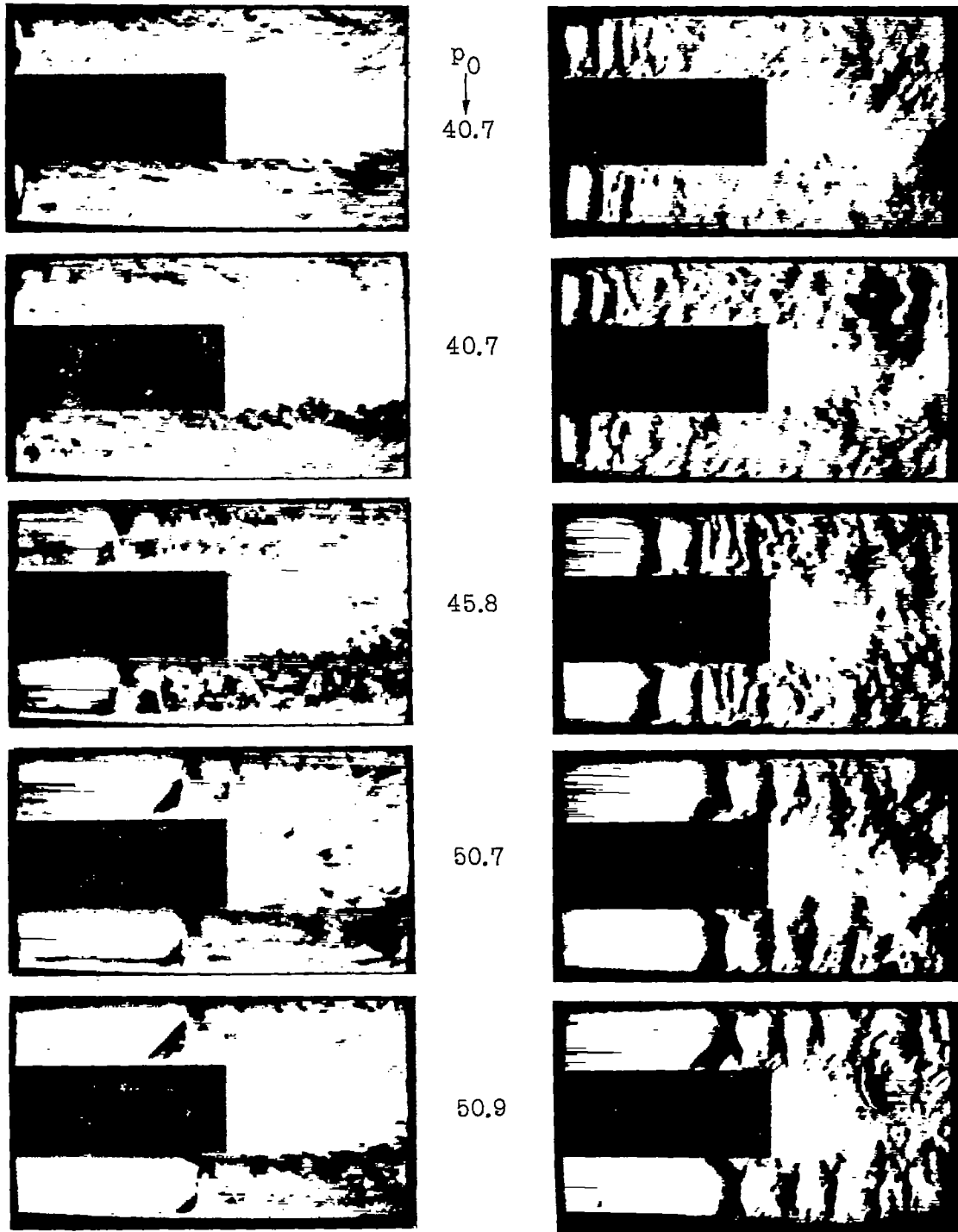


Figure 12.- Schlieren photographs of the outer streams over a two-dimensional base without a splitter plate at various stagnation pressures.

L-83313

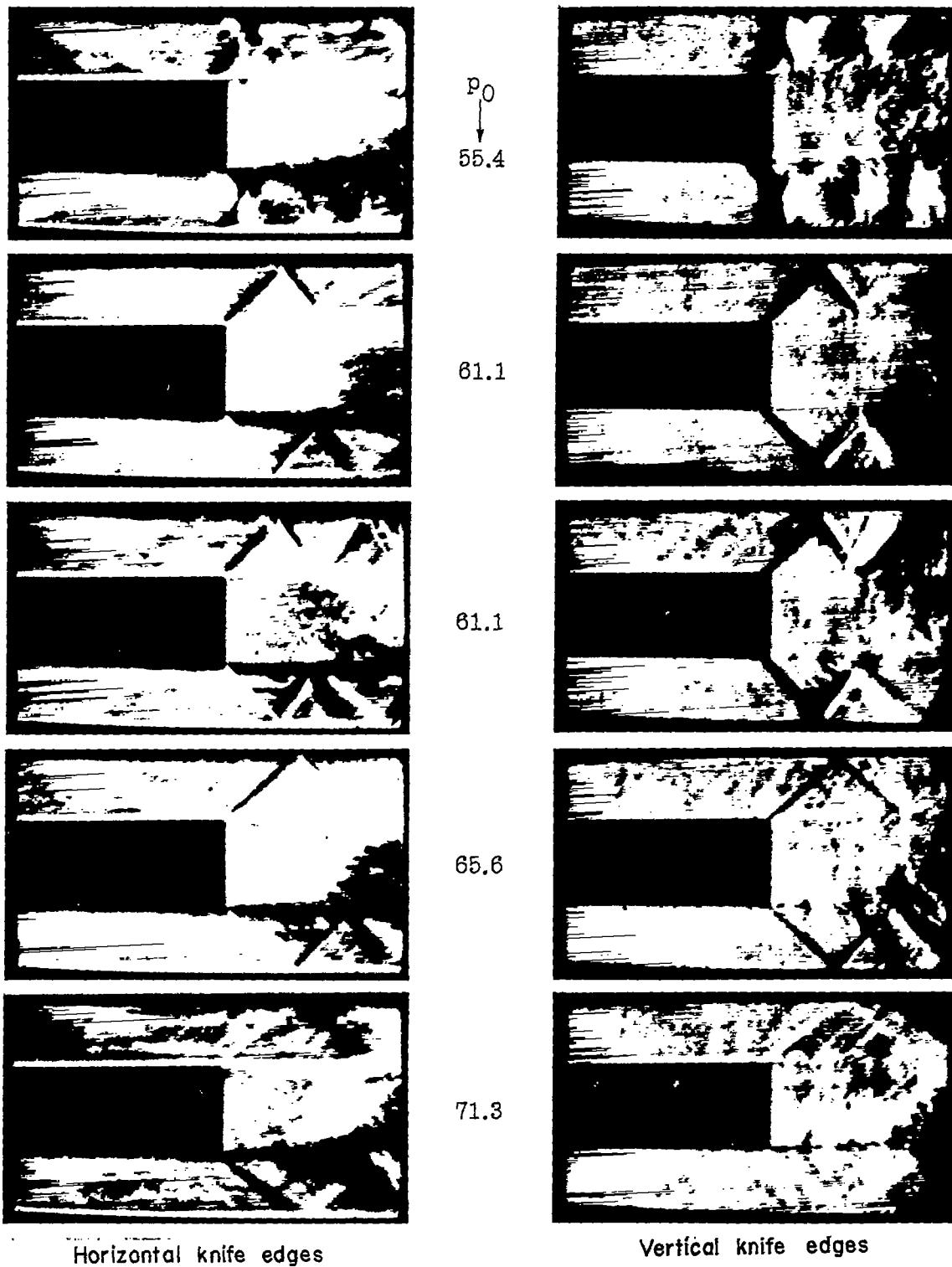


Horizontal knife edges

Vertical knife edges

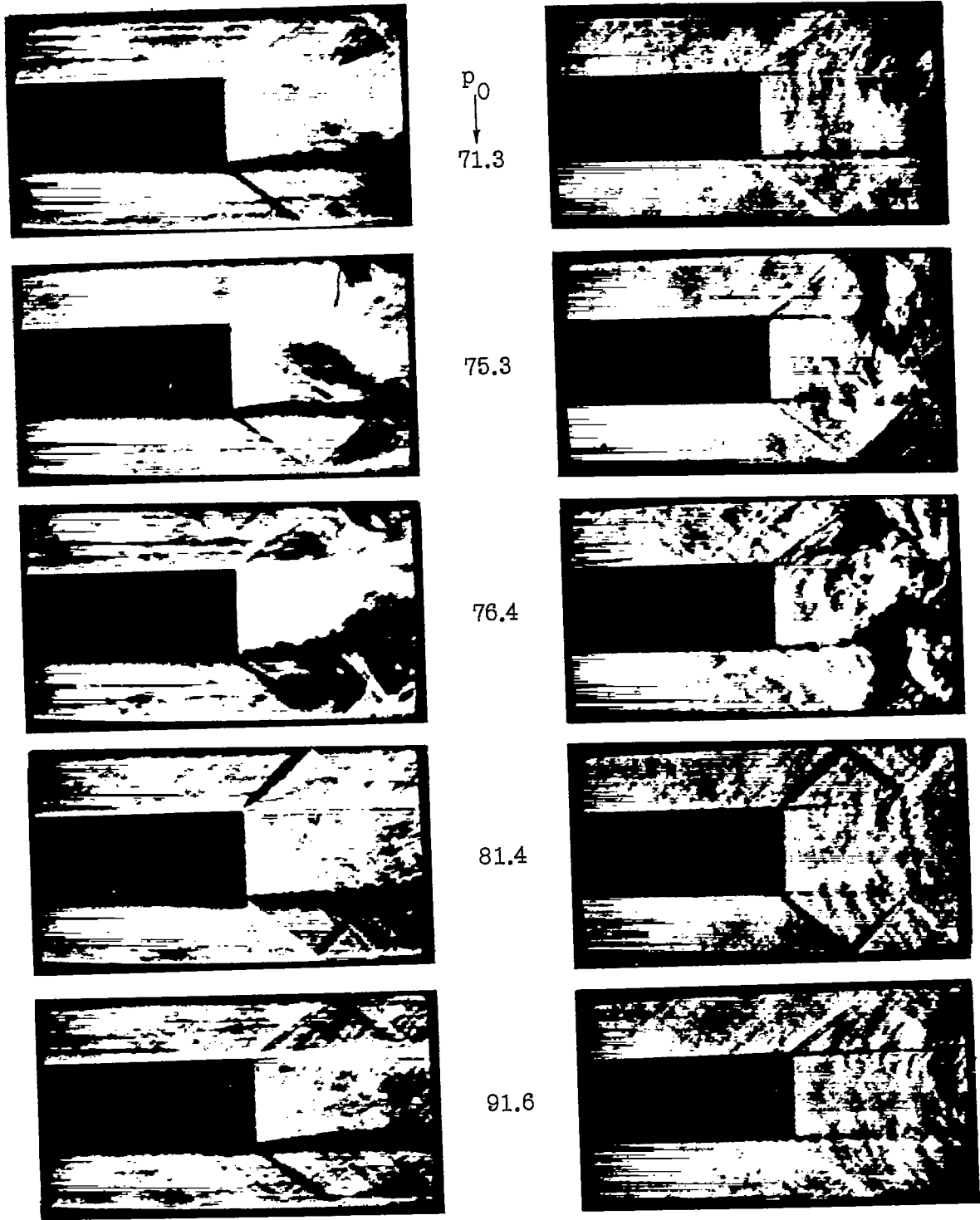
L-83314

Figure 12.- Continued.



L-83315

Figure 12.- Continued.

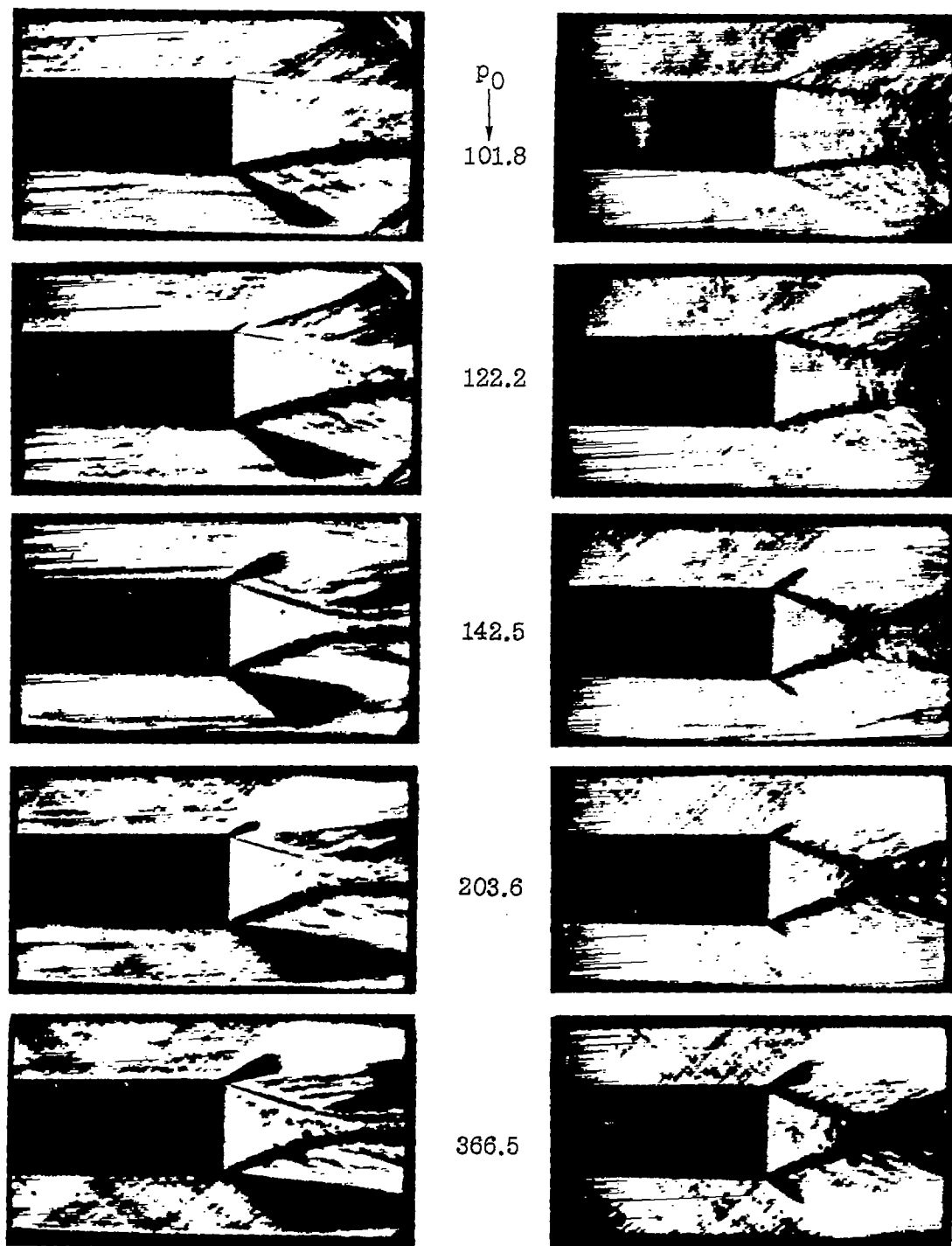


Horizontal knife edges

Vertical knife edges

L-83316

Figure 12.- Continued.

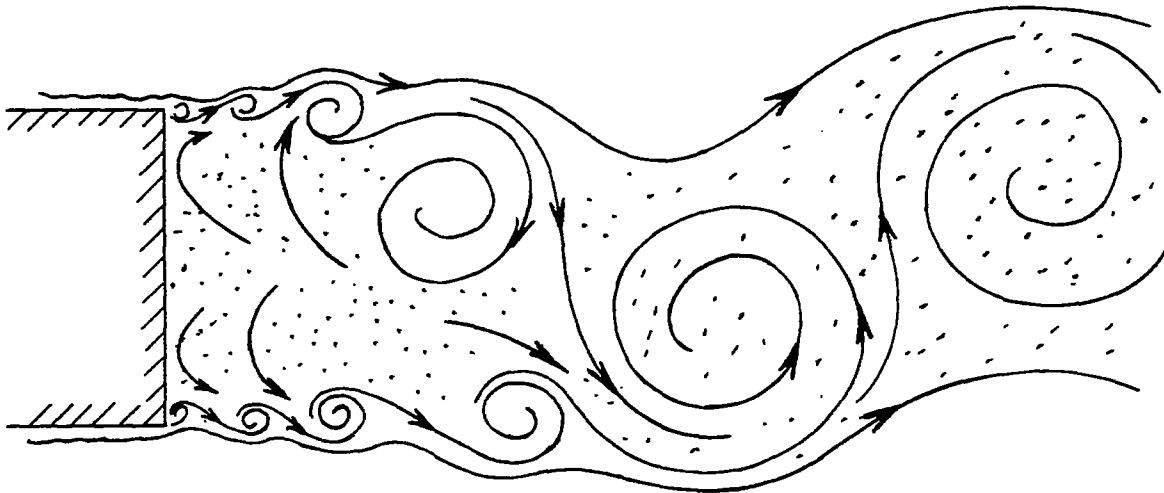


Horizontal knife edges

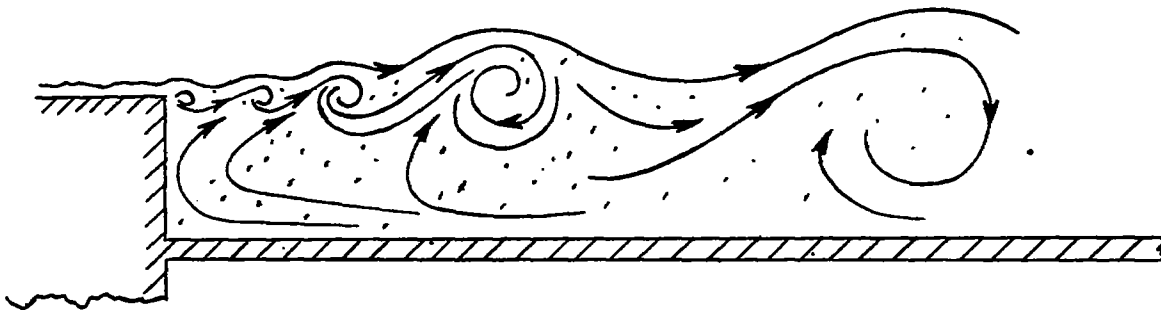
Vertical knife edges

L-83317

Figure 12.- Concluded.

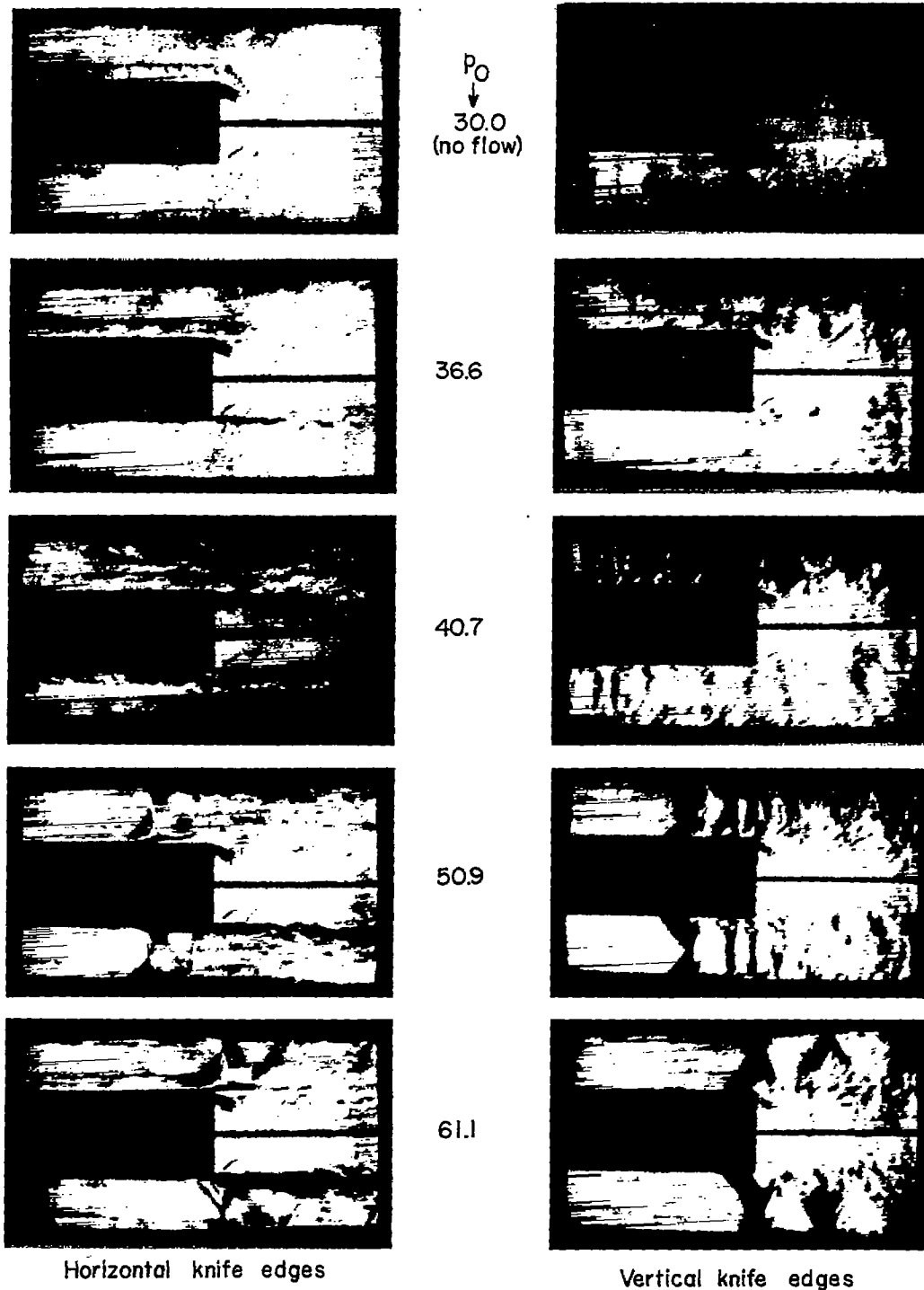


(a) No splitter plate.



(b) With splitter plate.

Figure 13.- Formation of the vortices behind two-dimensional base at subsonic speeds with and without splitter plate ( $p_0$  35 to 40 inches of mercury absolute).



L-83318

Figure 14.- Schlieren photographs of the outer streams over a two-dimensional base with a 1/16-inch-thick splitter plate at various stagnation pressures.

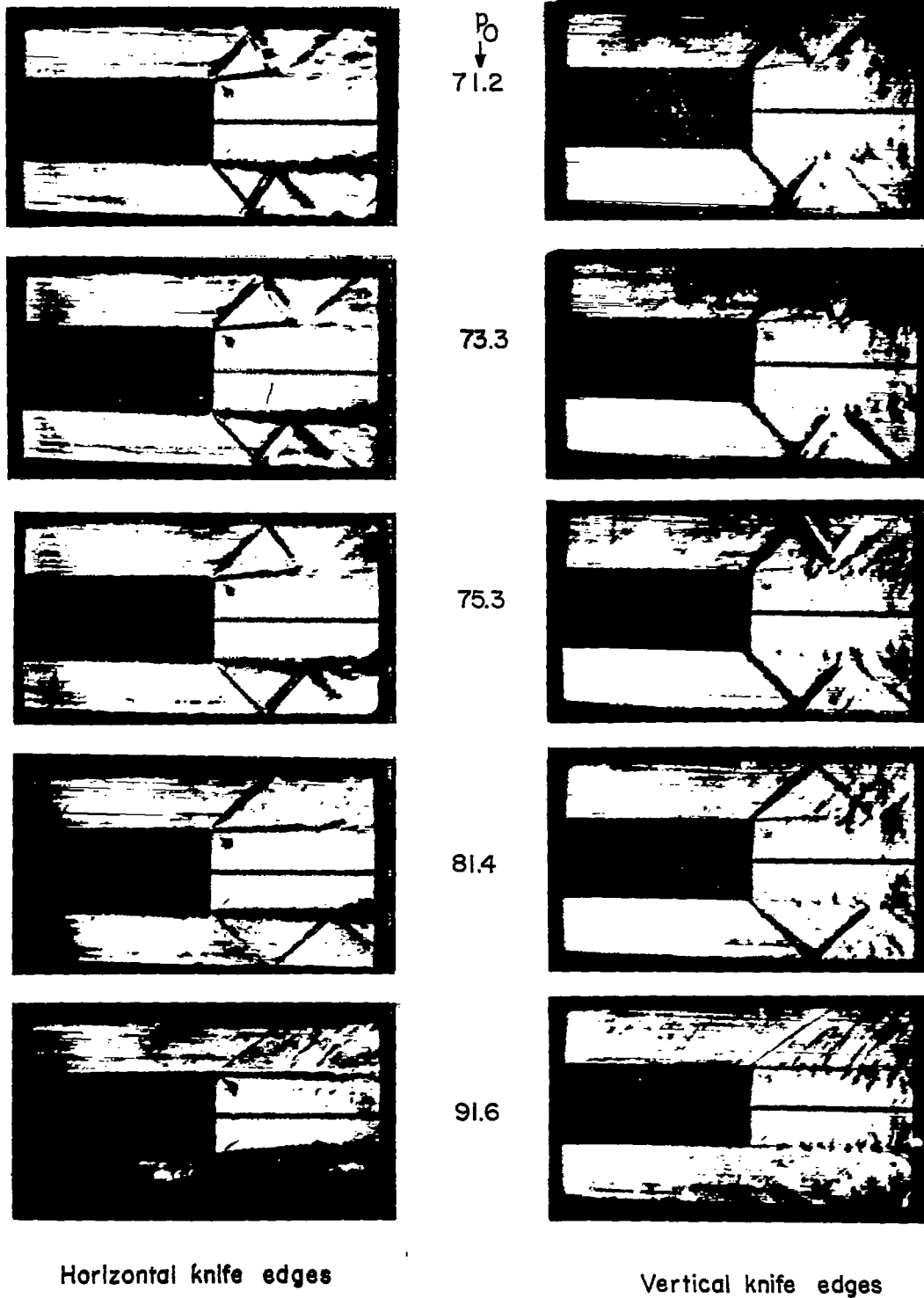
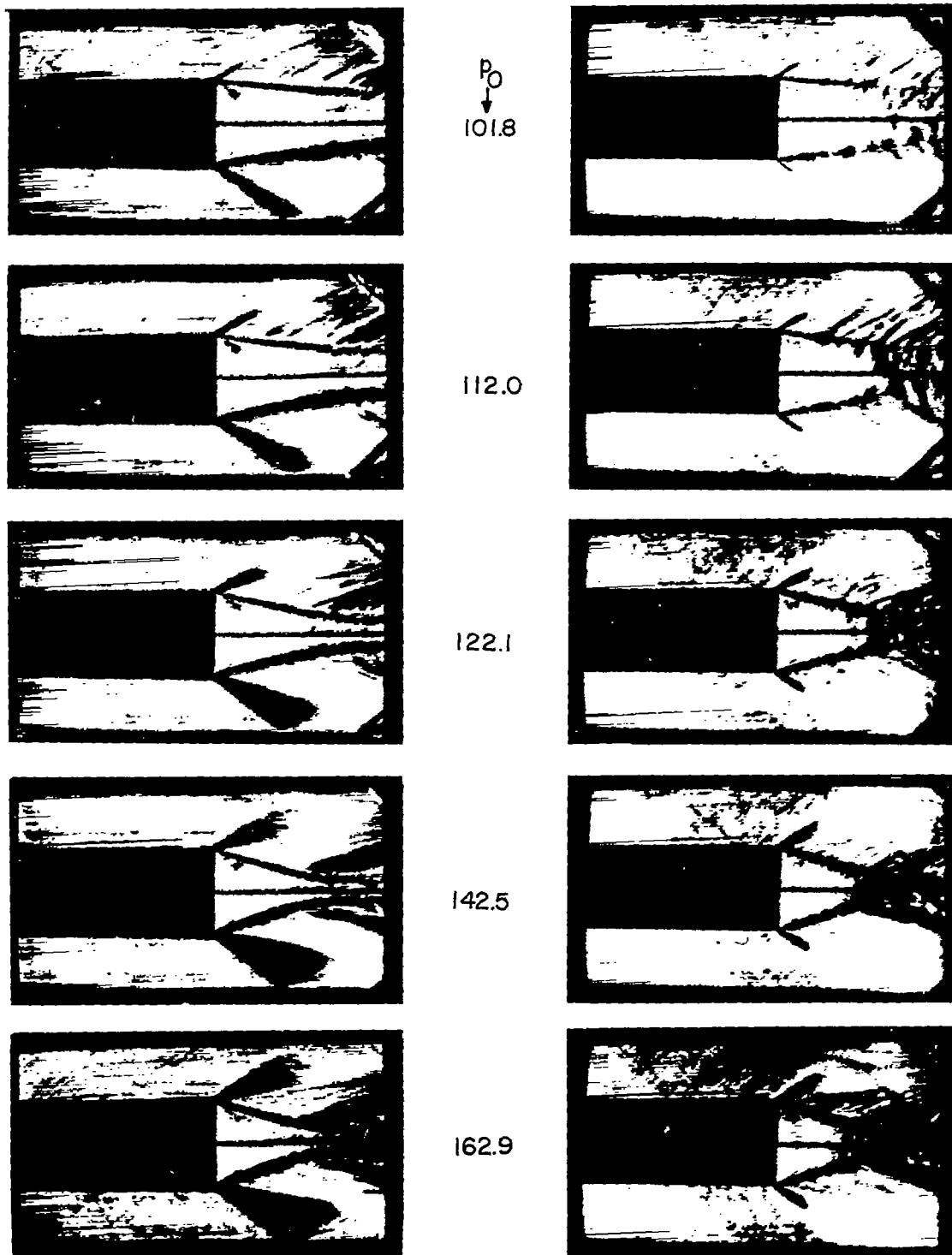


Figure 14.- Continued.

L-83319

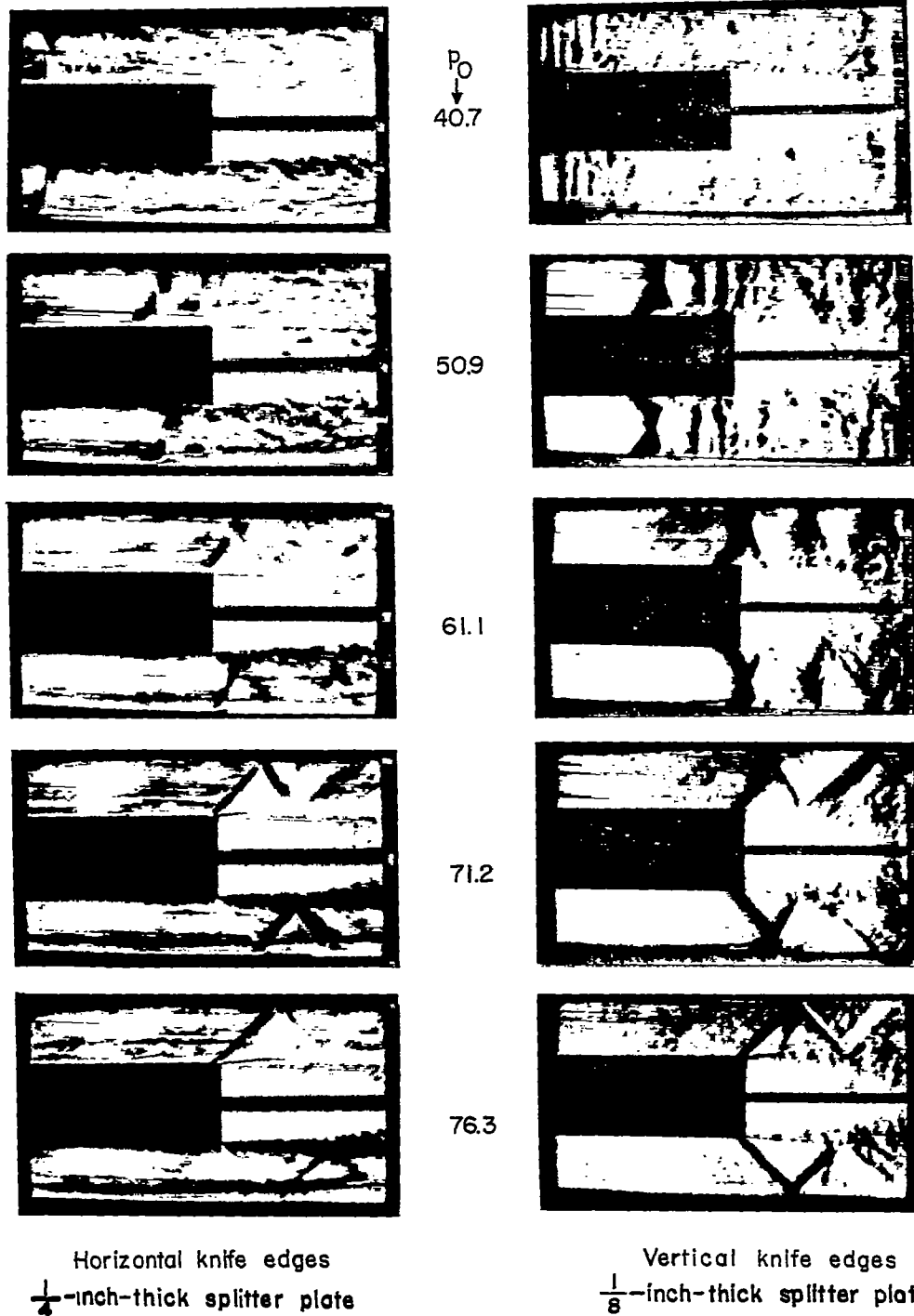


Horizontal knife edges

Vertical knife edges

L-83320

Figure 14.- Concluded.



L-83321

Figure 15.- Schlieren photographs of the outer streams over a two-dimensional base with a  $\frac{1}{4}$ - and  $\frac{1}{8}$ -inch-thick splitter plates at various stagnation pressures.

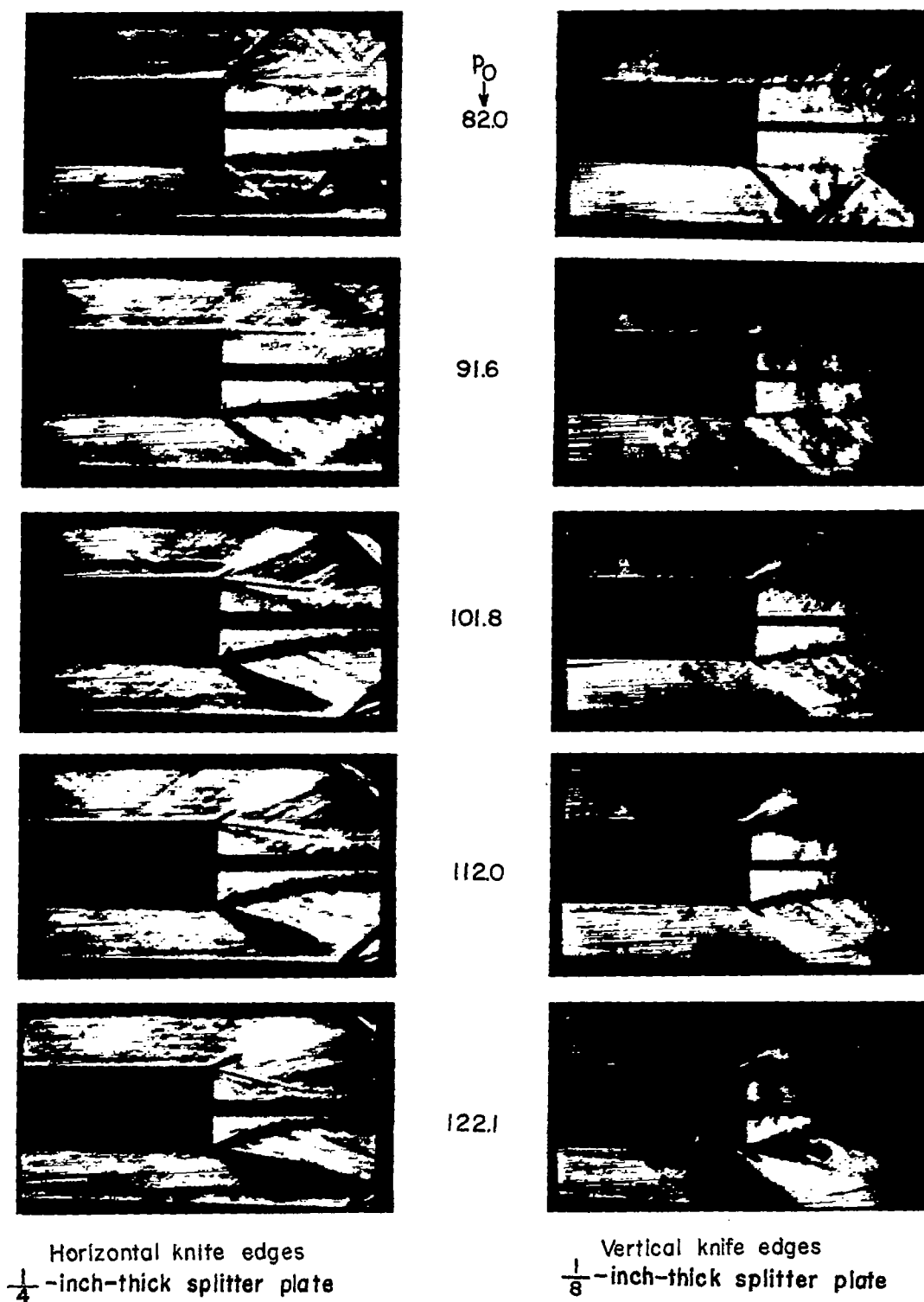


Figure 15.- Concluded.

L-83322

- 1/4 inch splitter plate
- ◇ 1/8 inch splitter plate
- △ 1/16 inch splitter plate

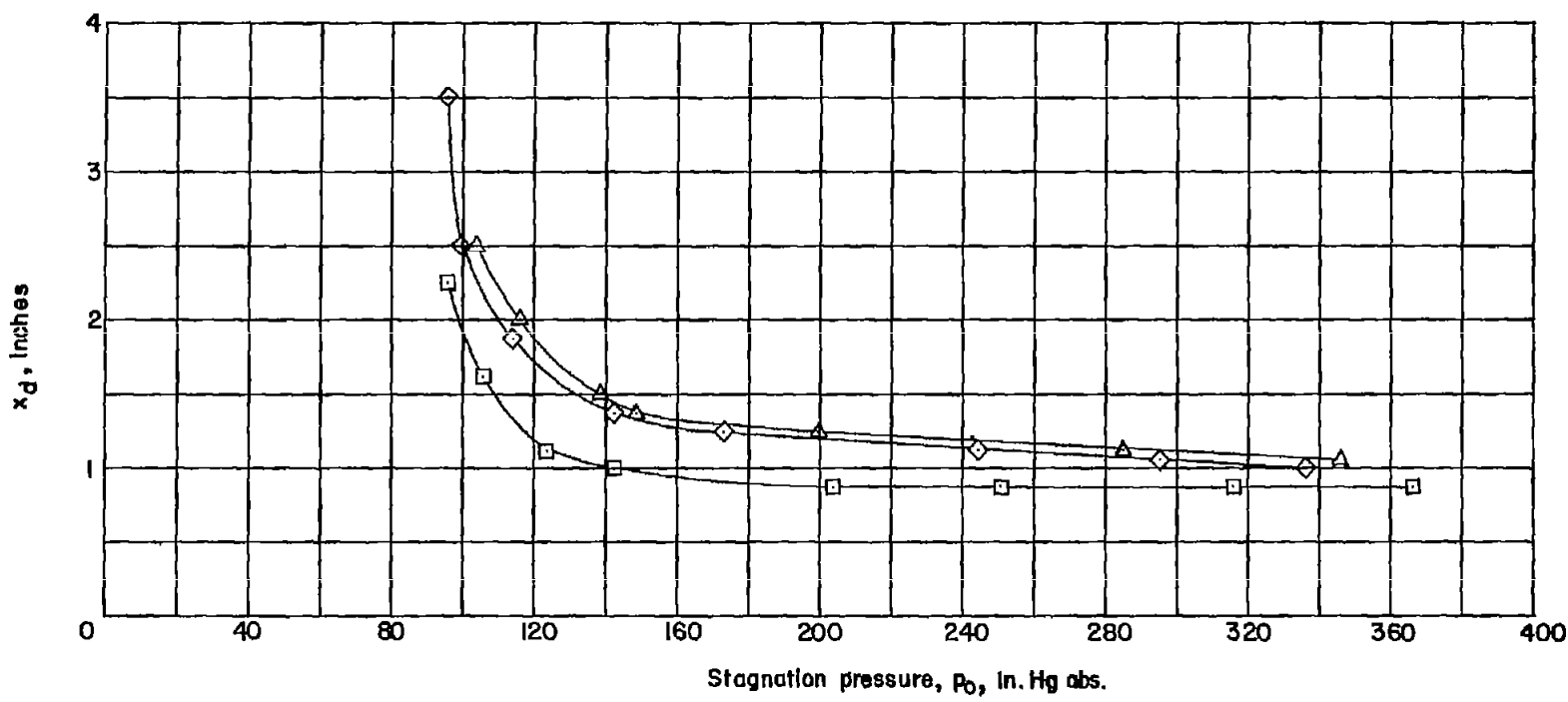
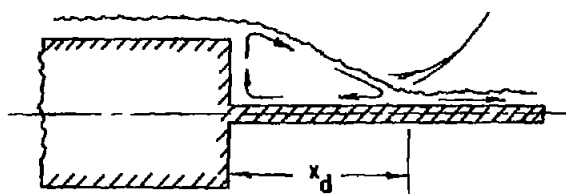
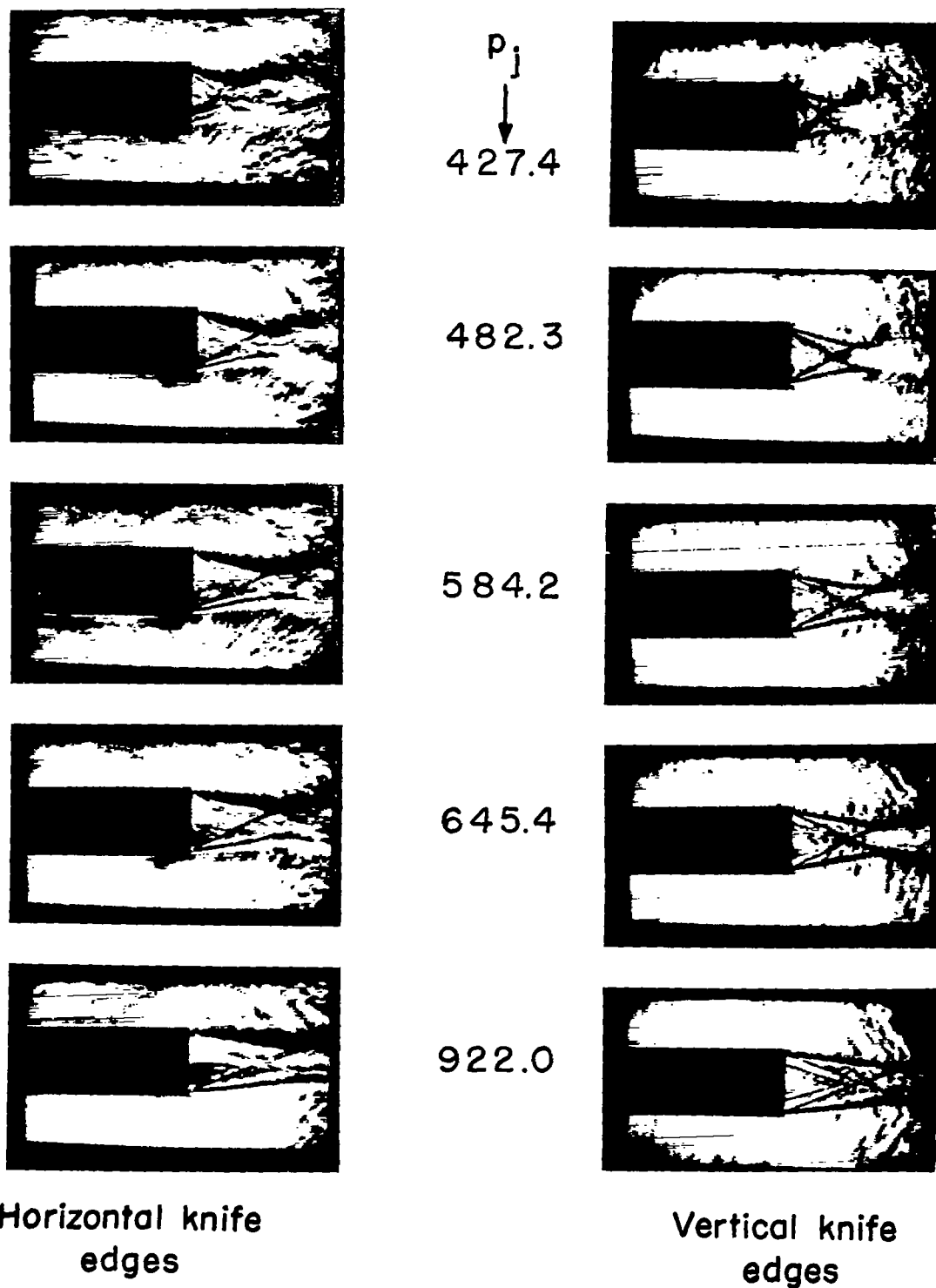


Figure 16.- Location of the division of the flow on the splitter plates.

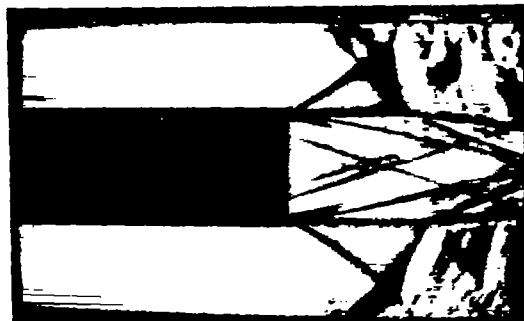
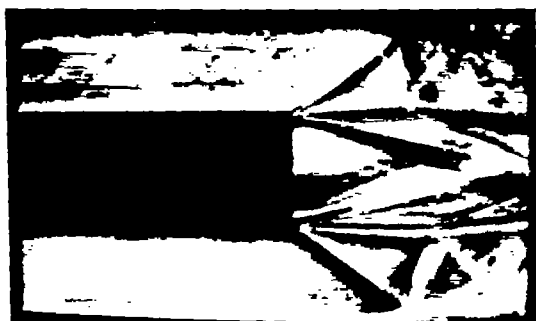


L-83323

Figure 17.- Schlieren photographs of the two-dimensional center jet at various stagnation pressures.



$p_0 = 55.0, p_j$  (no flow)



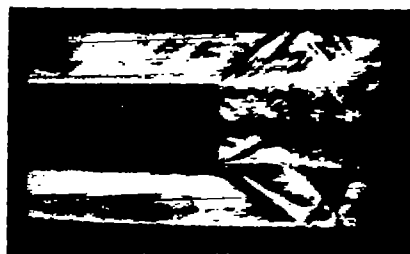
Horizontal knife edges

Vertical knife edges

$p_0 = 55.0, p_j = 906.0$

L-83324

Figure 18.- Schlieren photographs showing the effect of the center jet on the outer streams.



$$p_0 = 61.1$$

$$p_j = 154.7$$



$$p_0 = 61.1$$

$$p_j = 205.6$$



$$p_0 = 61.1$$

$$p_j = 238.2$$



$$p_0 = 61.1$$

$$p_j = 274.8$$



$$p_0 = 61.1$$

$$p_j = 299.3$$

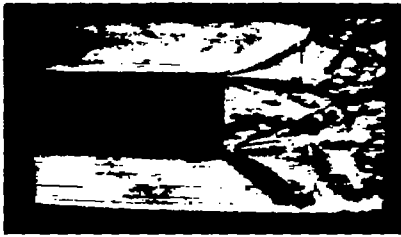


Horizontal knife  
edges

Vertical knife  
edges

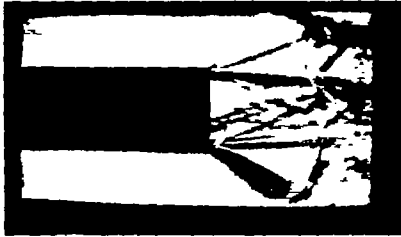
L-83325

Figure 19.- Schlieren photographs of the phenomena associated with the interaction of the outer streams and center jet for a constant outer-stream stagnation pressure and a variable center-jet stagnation pressure.



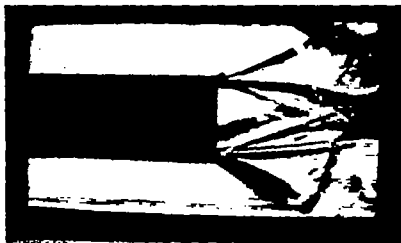
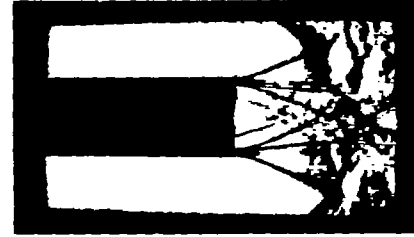
$$p_o = 61.1$$

$$p_j = 344.1$$



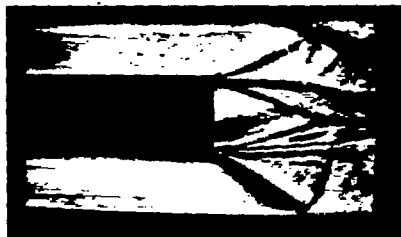
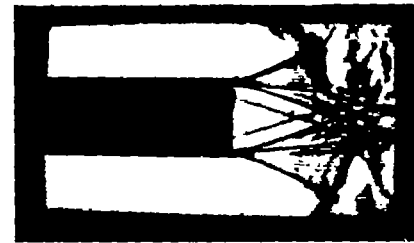
$$p_o = 61.1$$

$$p_j = 392.9$$



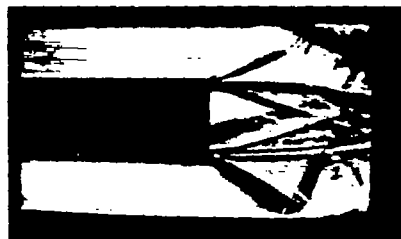
$$p_o = 61.1$$

$$p_j = 437.7$$



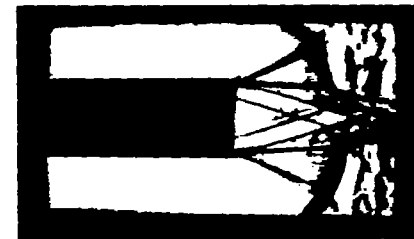
$$p_o = 61.1$$

$$p_j = 529.3$$



$$p_o = 61.1$$

$$p_j = 559.9$$

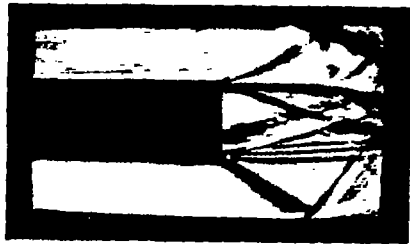


Horizontal knife  
edges

Vertical knife  
edges

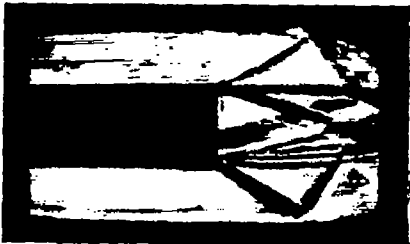
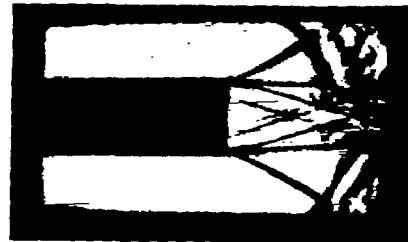
L-83326

Figure 19.- Continued.



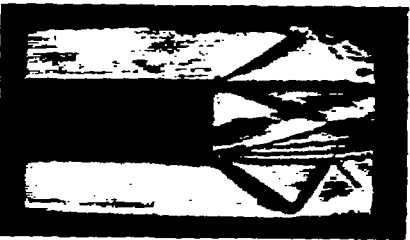
$$p_0 = 61.1$$

$$p_j = 627.0$$



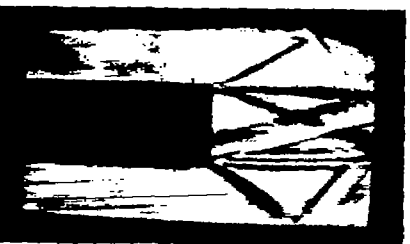
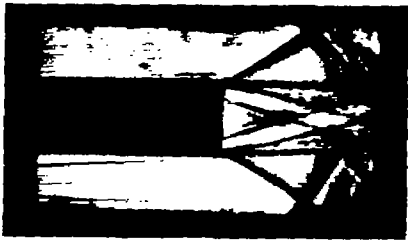
$$p_0 = 61.1$$

$$p_j = 722.7$$



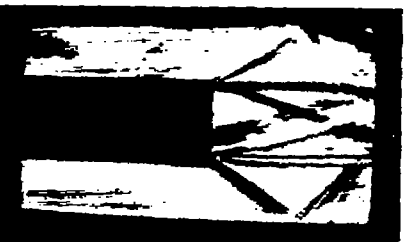
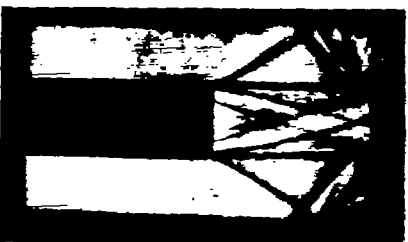
$$p_0 = 61.1$$

$$p_j = 753.3$$



$$p_0 = 61.1$$

$$p_j = 787.9$$



$$p_0 = 61.1$$

$$p_j = 824.5$$

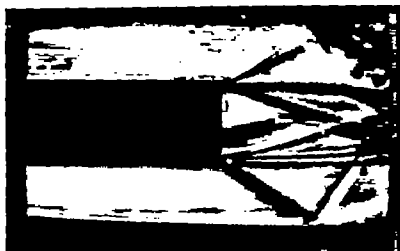


Horizontal knife  
edges

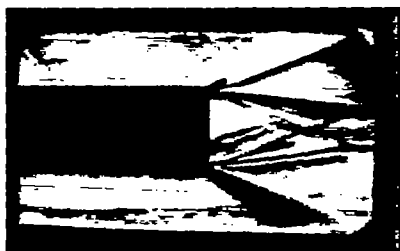
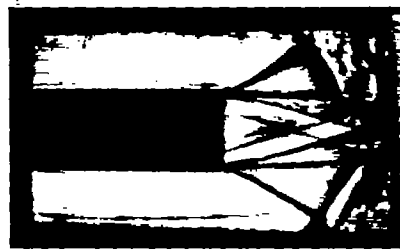
Vertical knife  
edges

Figure 19.- Concluded.

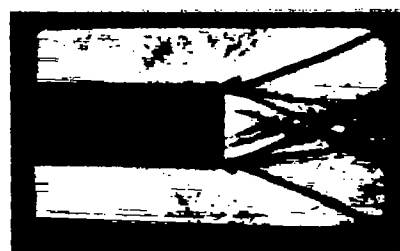
L-83327



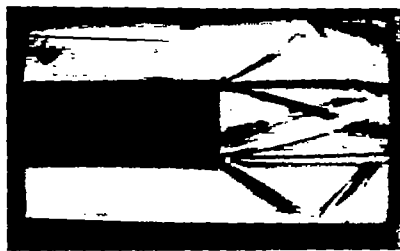
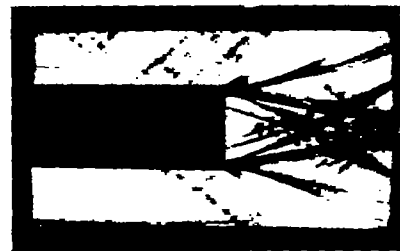
$p_0 = 61.1$   
 $p_j = 682.0$



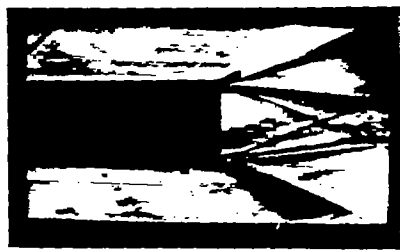
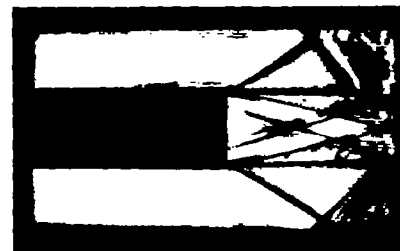
$p_0 = 122.1$   
 $p_j = 682.0$



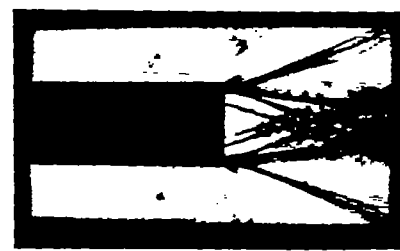
$p_0 = 173.0$   
 $p_j = 688.1$



$p_0 = 61.1$   
 $p_j = 824.5$



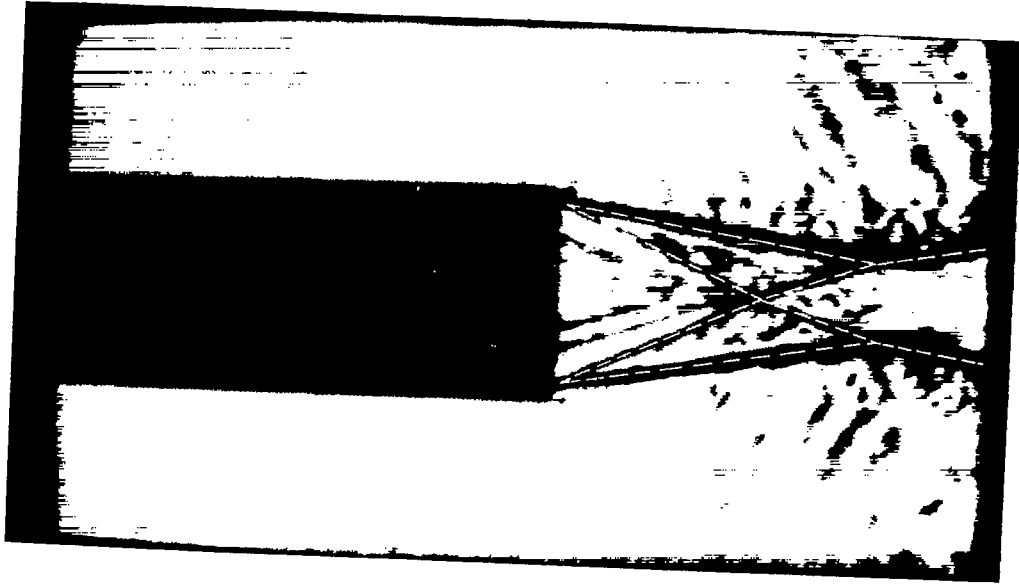
$p_0 = 148.6$   
 $p_j = 824.5$



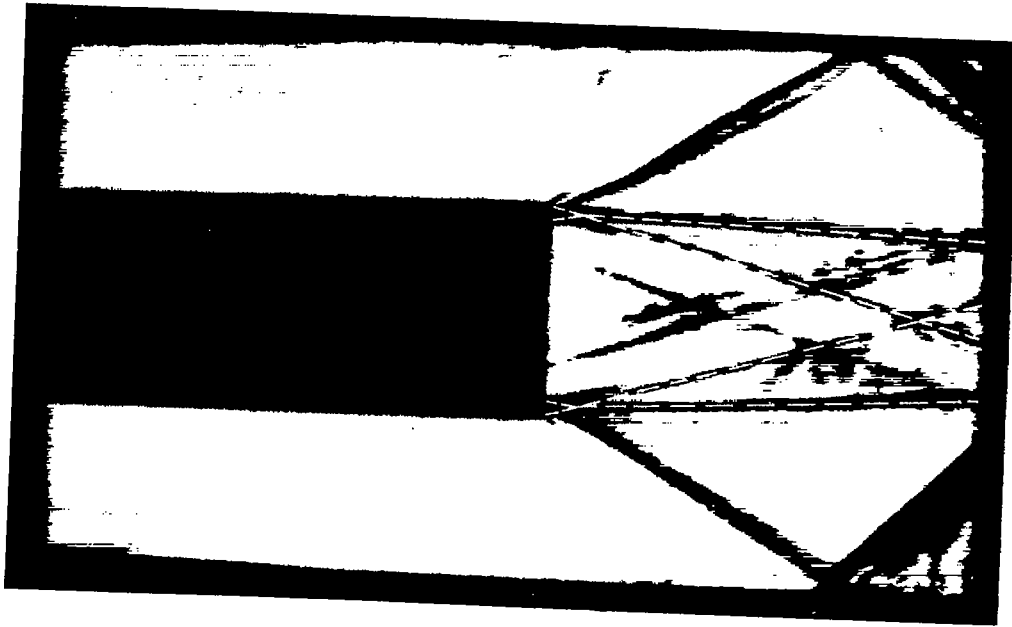
Horizontal knife  
 edges

Vertical knife  
 edges L-83328

Figure 20.- Schlieren photographs of the phenomena associated with the interaction of the outer streams and center jet for two cases of approximately constant center-jet stagnation pressures and variable outer-stream stagnation pressure.



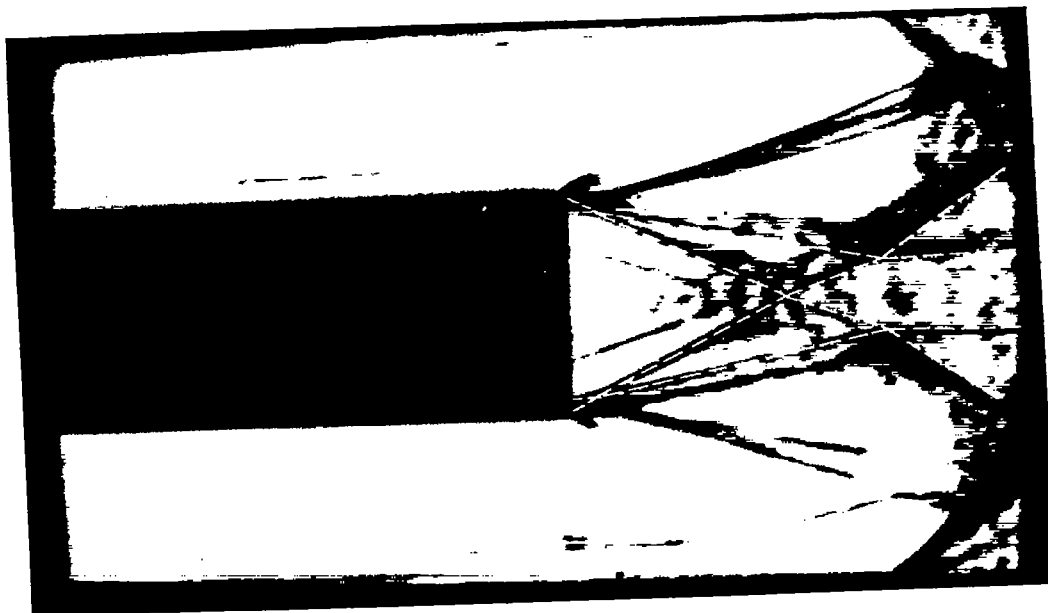
(a)  $p_0 = 30.0$  (no flow);  
 $p_j = 755.0$ .



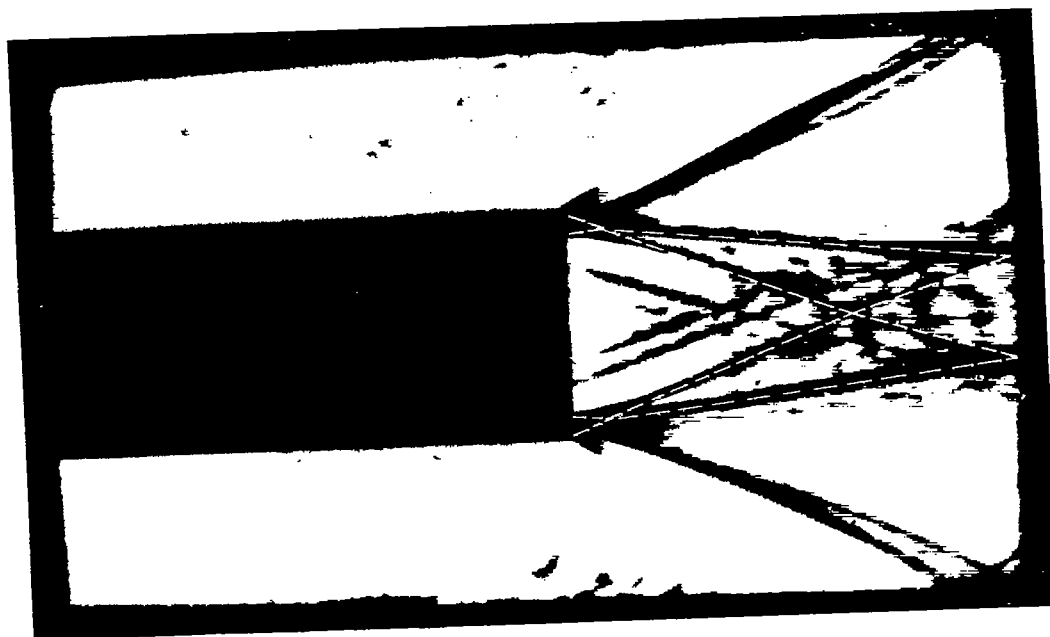
(b)  $p_0 = 71.2$ ;  
 $p_j = 808.2$ .

Figure 21.- Theoretical shock patterns of the two-dimensional flow superimposed on schlieren photographs obtained in the mixing-zone apparatus.

L-83329



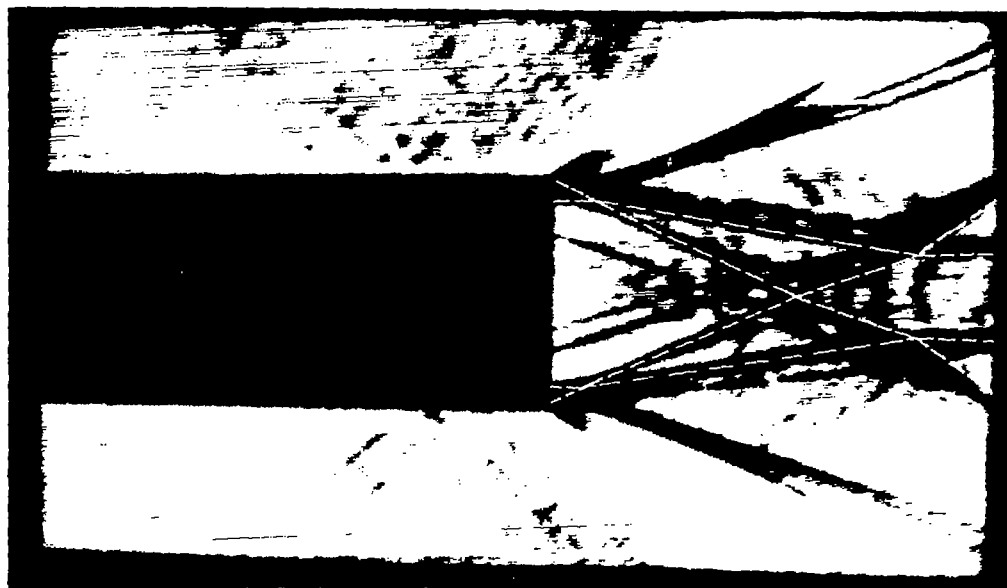
(c)  $p_0 = 101.8$   
 $p_j = 360.3$



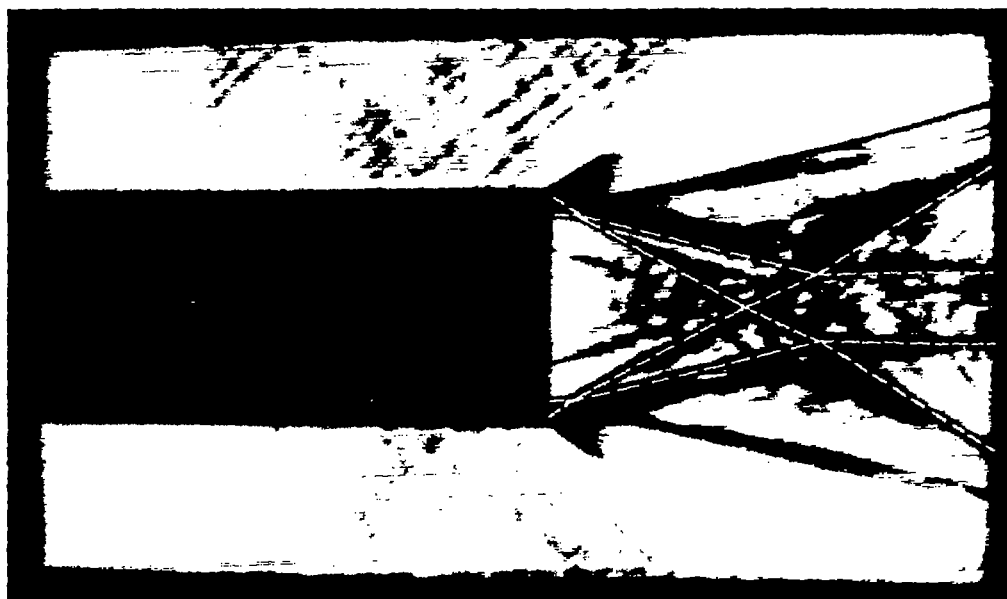
(d)  $p_0 = 132.3$   
 $p_j = 891.7$

L-83330

Figure 21.- Continued.



(e)  $p_0 = 160.8;$   
 $p_j = 763.4.$



(f)  $p_0 = 223.9;$   
 $p_j = 580.2.$

L-83331

Figure 21.- Concluded.

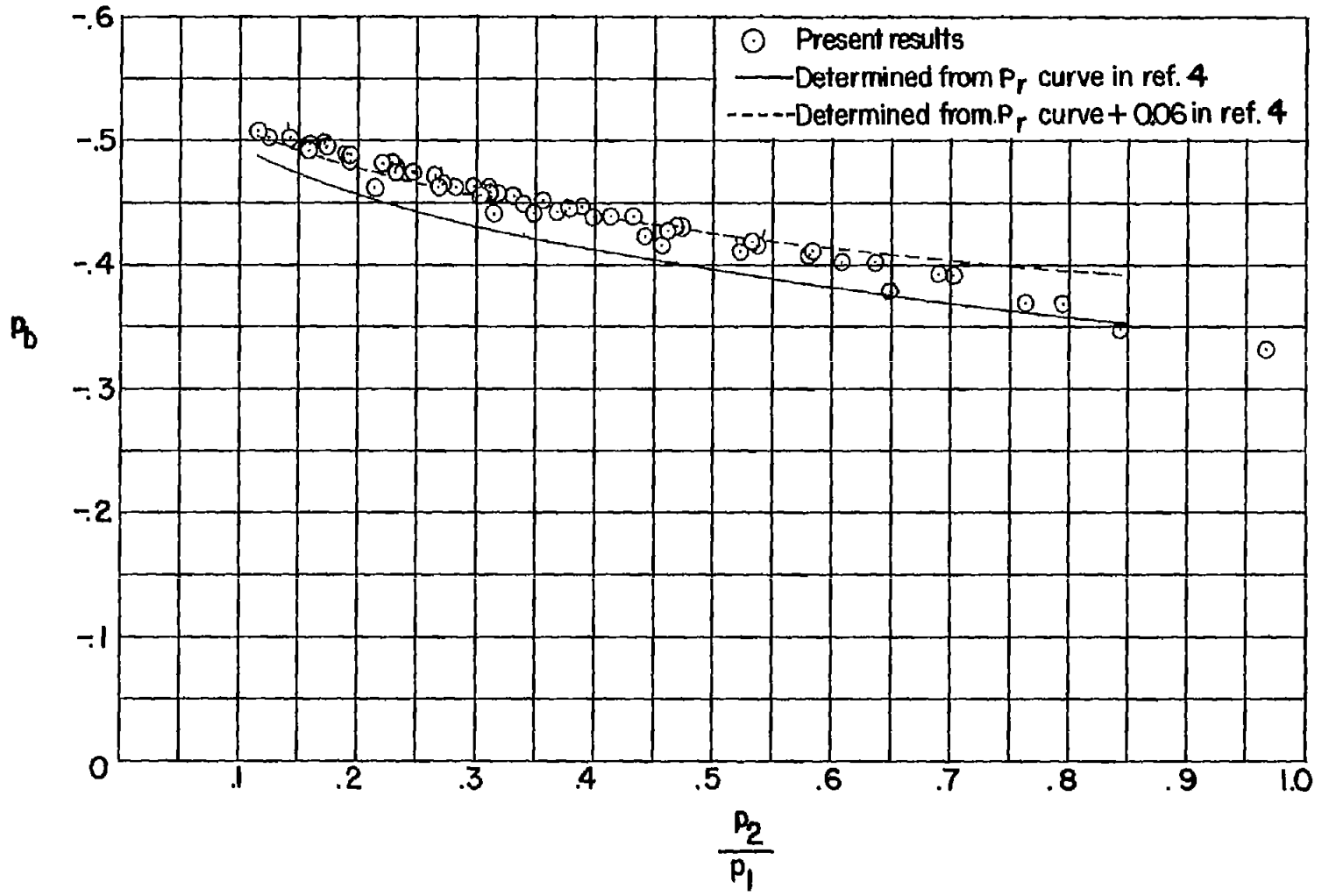
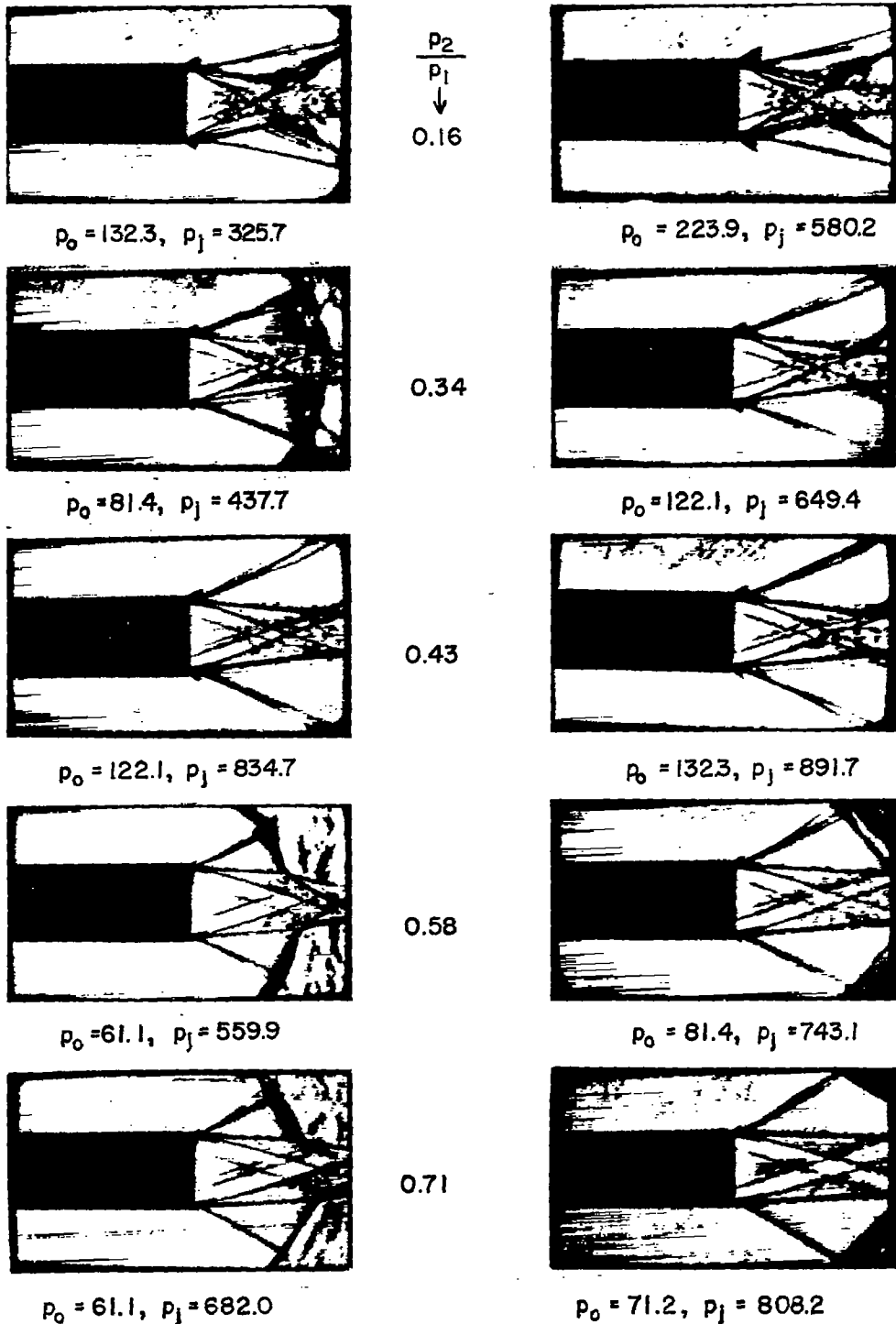


Figure 22.- Variation of two-dimensional base-pressure coefficient as a function of the ratio of static pressures of the center jet to the outer stream. Flagged symbols denote check values.



L-83332

Figure 23.- Comparison of the flows in the vicinity of the base for constant ratios of  $p_2/p_1$  with varying  $p_0$  and  $p_j$  values. (Vertical-knife-edge schlieren photographs.)

~~Handwritten scribble~~  
57-2143